Fine–scale structure in cometary dust tails II: further evidence for a solar wind influence on cometary dust dynamics from the analysis of striae in comet C/2011 L4 Pan-STARRS

Fine–Scale Structure in Cometary Dust Tails II: Further Evidence for a Solar Wind Influence on Cometary Dust Dynamics from the Analysis of Striae in Comet C/2011 L4 Pan-STARRS

Oliver Price[a,b], Geraint H. Jones[a,b], Karl Battams[c], Mathew Owens[d]

[a]*Mullard Space Science Laboratory, Department of Space & Climate Physics, University College London, Holmbury St. Mary, Dorking, Surrey RH5 6NT, UK*
[b]*The Centre for Planetary Sciences at UCL/Birkbeck, London, UK*
[c]*Naval Research Laboratory, Washington, D. C., USA*
[d]*Space and Atmospheric Electricity Group, Department of Meteorology, University of Reading, UK*

Abstract

Striated features, or *striae*, form in cometary dust tails due to an as-yet not fully constrained process or processes. Using STEREO-B SECCHI HI-1 instrument data, we display the evolution of striae in the tail of C/2011 L4 over a period of 8 days. This includes a period of morphological changes on 2013 March 14-15, similar to the reorganisation of striae observed in the tail of C/2006 P1. This reorganisation is again attributed to Lorentz forces caused by the comet's dust tail crossing the heliospheric current sheet. We further analyse the alignments of reorganised striae at both C/2006 P1 and C/2011 L4 and show these alignments have mixed compatibility with an additional solar wind influence. We also report the discovery of a bright neutral sodium tail at C/2011 L4.

Highlights

- Striae are shown to remain at the same locations in temporal maps over time, further demonstrating the accuracy of the temporal mapping technique.
- The mapping technique highlights a period of morphological change during 2013 March 14-15, which we argue from a comparison with solar wind simulations is from changing Lorentz force effects on dust grains as they cross the heliospheric current sheet; a similar phenomenon to that observed in the tail of C/2006 P1.
- We examine whether the alignments of reorgnanised striae at both C/2006 P1 and C/2011 L4 are consistent with solar wind features moving through the tail at speeds comparable to those predicted by such solar wind simulations.
- We report the presence of a bright neutral sodium tail at C/2011 L4.

Keywords: Comets, dust, Comets, plasma, Solar wind

1. Introduction

Comet dust grains' trajectories are influenced by solar radiation pressure to form (type II) dust tails, which lag behind the nucleus's motion about its orbit, e.g. Fulle (2004). Features observed in such tails include *synchronic bands*, which are large-scale linear features that are coaligned with the position of the comet's nucleus, and *striae*. The latter are features that have only been observed in a few, generally very high production rate comets, including C/1957 P1 Mrkos (Sekanina, Z, Farrell, 1982), C/1962 C1 Seki-Lines (McClure, 1962), C/1975 V1 West (Koutchmy and Lamy, 1978; Lamy and Koutchmy, 1979; Nishioka et al., 1992), C/1996 O1 Hale-Bopp (Sekenina and Pittichová,

Email address: g.h.jones@ucl.ac.uk ()

1997), C/2006 P1 McNaught (Price et al., 2019), and C/2020 F3 NEOWISE. Although several processes for striae formation have been proposed, we lack a universally-accepted one. Price et al. (2019) presented the first image sequences that record the formation of striae. Strong evidence was also presented that striae can be modified after their formation, and that the heliospheric magnetic field embedded within the solar wind could be responsible for these changes.

Here, we follow up the work presented in Price et al. (2019), by analysing the striae-rich dust tail belonging to C/2011 L4 Pan-STARRS (from here on referred to as *C/2011 L4* only), and compare similarities in highly striated dust tail behaviours at both C/2011 L4 and C/2006 P1. The temporal mapping technique outlined in Price et al. (2019) was used in this analysis, which again demonstrates its ~~great~~ value in deciphering the evolving nature of dust tails in a consistent manner.

To investigate the dust tail at C/2011 L4, we make use of a sequence of images captured by the *Heliospheric Imager* (*HI*) that forms part of the wider *Sun-Earth Connection Coronal and Heliospheric Investigation* (*SECCHI*) remote sensing package on the NASA *STEREO-B* spacecraft. The formation and evolving appearance of numerous striae is tracked, including the progressive realignment of many striae. Using solar wind simulations, we show that this reorganisation correlates with two crossings of the heliospheric current sheet (HCS) in quick succession. We attribute changes in dust dynamics to interactions between electrically charged dust grains and the heliospheric magnetic field, as was also observed and simulated at C/2006 P1 by Price et al. (2019).

We revisit the tail of C/2006 P1 using the *HI-1* dataset from *STEREO-A*, and compare the reorganisation events at both comets. In particular we further analyse new features at both comets which are observed to only appear once the reorganisation has begun. We investigate whether the orientation of these features is consistent with a solar wind source moving through each comet tail at a speed consistent with the solar wind speeds predicted by simulations. Finally, we also model the behaviour of two other tails of C/2011 L4 present within the *STEREO-B* dataset. Our analysis indicates that one of these tails is the (type I) ion tail, and the other a previously unidentified bright neutral sodium tail.

1.1. C/2011 L4 Pan-STARRS

The comet of primary interest in this work was discovered on the 6th June 2011 by the Panoramic Survey Telescope and Rapid Response System (Pan-STARRS), located at Haleakala observatory in Hawaii (Wainscoat et al., 2011). Then 7.9 AU from the sun at an apparent magnitude of +19, it eventually became visible to the naked eye around its perihelion on 2013 March 10 04:05, at 0.302 AU from the sun.

Combi et al. (2014) found the water production of C/2011 L4 to follow the relationship $1.3 \times 10^{29} r^{-1.3}$ s^{-1} before perihelion and $5.0 \times 10^{28} r^{-2.3}$ s^{-1} after perihelion, where r is heliocentric distance, with a maximum water production rate of $1{\times}10^{30}$ molecules s^{-1}. This higher pre-perihelion activity, the comet's secular light curve (Ferrín, 2014), and its orbital parameters, are consistent with C/2011 L4 being a dynamically new Oort cloud comet passing through the solar system for the first time. Multi-wavelength observations of C/2011 L4 showed it to be unusually dust rich (Yang et al., 2014).

1.2. Striae Formation Theories

We refer the reader to Price et al. (2019) for a full background to striae formation theories. In brief, most striae models describe formation through the fragmentation of larger dust particles. In addition to gravity, cometary dust grains are strongly influenced by radiation pressure. As these two primary forces act in opposition to each other and both follow inverse square laws, the effective force acting on them is equivalent to *reduced gravity*. This is parametrised by the dimensionless constant β_r (we denote β_r to avoid confusion with, e.g., plasma β), given as:

$$\beta_r = \frac{\text{Radiation Force}}{\text{Gravitation Force}} \tag{1}$$

The fragmentation of grains leads to the spreading of dust grains over time due to a difference in the β_r parameter between individual particles.

Sekanina and Farrell (1980) proposed a two-step process. Clouds of parent particles with similar β_r values quickly break up into daughters particles with a range of β_r values. This provides a good match to observational data (Pittichová et al., 1997), but the required physical properties of dust are difficult to explain. Nishioka and Watanabe (1990),

Nishioka (1998) and Nishioka (2021) instead suggest a continuous cascade of striae formation, which relaxes the constraints on dust properties, but has alleged problems explaining stria shapes (Sekenina and Pittichová, 1997). Other potential mechanisms include optically thick dust clouds (Froehlich and Notni, 1988; Notni and Thaenert, 1988), or the destruction of macroscopic sized (10 - 100m) boulders by rotational stresses (Steckloff and Jacobson, 2016).

In Price et al. (2019), a sequence of images of C/2006 P1 from the SOHO LASCO C3 instrument using its Blue filter showed directly the formation of striae. These images show that striae form on timescales of 6 to 9 hours as juxtaposed regions that both brighten and darken, and that striae do not always form in the same order by which the constituent dust within them was released from the nucleus. Some striae form with linear morphologies aligned directly towards/away from the sun, which may indicate that shadowing effects might play a role in their creation as described by Froehlich and Notni (1988). However, not all striae form in this way, with some having a curved orientation relative to this antisunward radial direction.

Lessons on striae formation were also ~~be~~ inferred from the way in which the striae were later disrupted at C/2006 P1 by their interaction with the heliospheric magnetic field. In this process each stria appears to be reorganised into many *interleaved* sections, rather than being shifted as a distinct entity. This would seem to indicate that each stria contains a more homogeneous distribution of β_r, rather than a strict ordering of β_r along its length. This result is in much better agreement with the Nishioka (1998); Nishioka and Watanabe (1990); Nishioka (2021) "cascade" striae formation model than the Sekanina and Farrell (1980) two-step process. We also note the most recent version of this model (Nishioka, 2021) is able to incorporate Lorentz force effects into its description of dust dynamics.

A more minor result was the detection within the STEREO-A HI-1 dataset of striated features which appear to "bridge" the gap between the main dust tail ($\beta_r \sim 1$) and the neutral iron tail ($\beta_r \sim 8$). Striated features at higher β_r had not been previously reported.

1.3. Motivations

One of the important results from Price et al. (2019) was the detection of a striae reorganisation phenomenon occurring at C/2006 P1. The dust tail appeared to undergo some process which disrupted the existing striae into *interleaved* sections. Simulations of the local solar wind conditions showed this phenomenon occured at the same time as the comet and its tail traversed the heliospheric current sheet, HCS, into an area of opposite magnetic polarity. It was hypothesized that a change in the direction of the Lorentz force acting on charged dust grains caused the reorganisation behaviour. HCS crossings having a noticeable effect on dust tail orientation was predicted by Horanyi and Mendis (1987). The observations presented by Price et al. (2019), together with those of Kramer et al. (2014), imply that Lorentz force effects can be a significant influence on dust tail morphology, and that grains strongly susceptible to electrodynamic forces are larger than had been previously anticipated. A goal of this work is to hopefully provide another 'data point' in this ongoing investigation.

Another unexpected result from the aforementioned paper is that many of the *interleaved* sections from the disrupted tail of C/2006 P1 eventually linked together to form new *striae-like* features. Figure 1 shows a section of C/2006 P1's dust tail as seen from STEREO-A HI-1, after the HCS crossing event has affected the whole of the dust tail. These new *striae-like* features clearly intersect the older striae, and in some cases stretch across the whole tail. We hereinafter refer to these features as *combed* striae. Whilst the original striae point roughly in the direction of the comet's nucleus (although not exactly, as they are not purely synchronic), the *combed* features point roughly towards/away from the sun.

Whilst the Lorentz force presents a good explanation for the disruption of the original striae features – and the correlation of events is convincing – there is no obvious explanation for how or why the disrupted features themselves should display any fine structure of the type that was clearly present.

Normal striae explanations of fragmentation also struggle to explain these new features, as the vast scale of the dust tail at the time of the disruption event (on the order of an astronomical unit) would make it unfeasible for fragmented dust of varying β_r to have spread out across such a vast distance in such a short period of time. It would therefore seem that some other aspect of the solar wind (accompanying the HCS crossing) must have been imprinting its structure on the dust tail. Another goal of this work is to investigate whether the alignment of these *combed* striae can give us any clues on the nature of their formation.

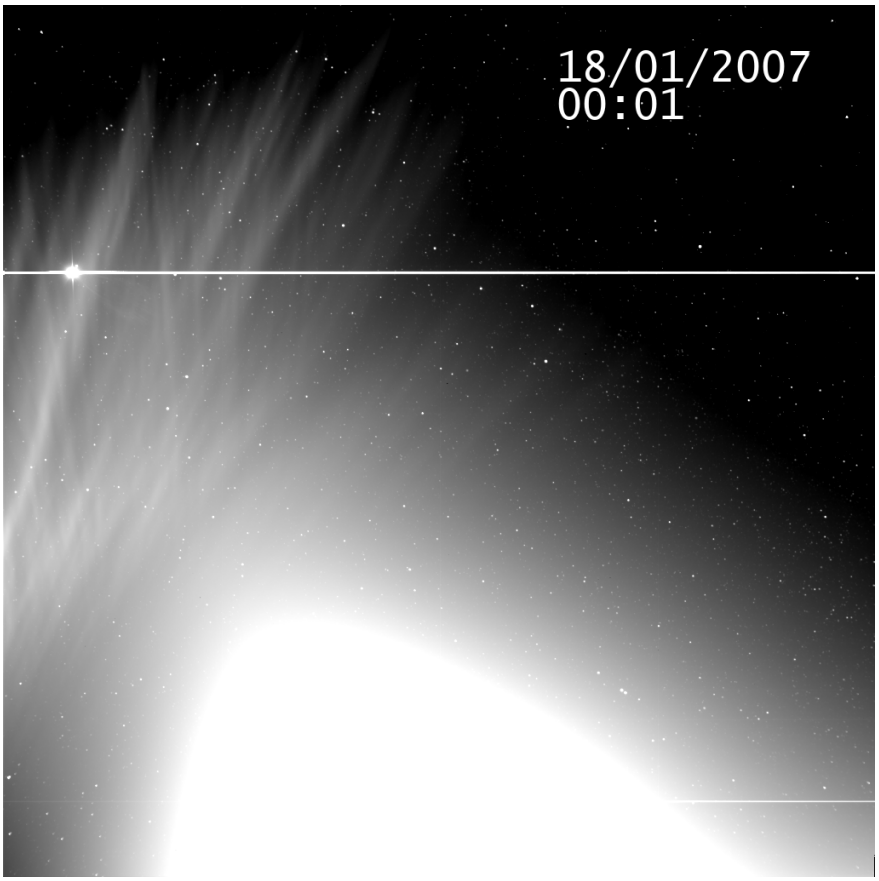

Figure 1: View of C/2006 P1 McNaught's dust tail from STEREO-A HI-1 (raw data), not presented in Price et al. (2019). The sun is outside the frame, towards the lower right (north approximately towards the right), and C/2006 P1 has exited the frame to the bottom left. The primary, original striae are visible as structures tilted in this view. Disrupted, "combed" striae features – near-vertical in this orientation – appear to form new structures that spread across the tail.

2. Data

Much like C/2006 P1 McNaught, C/2011 L4 was fortunately also observed by the HI instruments aboard the STEREO spacecraft. The main data source used here to study C/2011 L4 is the STEREO-B HI-1 instrument, part of the SECCHI suite of instuments (Howard et al., 2008), which imaged the comet and its tail during and shortly after perihelion. The far reaches of the comet's tail were also captured by HI-2, and the comet was also captured once by STEREO-A. C/2011 L4 was not as active as C/2006 P1 and there not as extensive within the HI field of view, although the nucleus remained in the field of view for longer.

Unfortunately the comet was not captured by the SOHO LASCO coronagraph; although useful data for the water production rates of the comet were taken by the SOHO Solar Wind Anisotropies (SWAN) instrument (Combi et al., 2014). Whilst the comet was also imaged from Earth, due to being fainter than C/2006 P1, the striae were much less apparent in any ground based images. The analysis of one such image is presented in Section 5.5, but this work's primary focus is the higher quality data captured by STEREO-B HI-1.

The HI-1 dataset was previously analysed by Raouafi et al. (2015) to investigate a phenomena they named *High-Velocity Evanescent Clumps* (HVECs), material that the authors suspected to be charged dust particles picked up by the solar wind or neutral atoms accelerated by radiation pressure with $\beta_r > 50$. However, other analyses have speculated that these clumps are simply the comet's ion tail (Ramanjooloo (2015); Ramanjooloo and Jones (2022)). Figure 2 shows the geometry of the Earth and various observing spacecraft relative to the comet and its tail during the SECCHI data collection period.

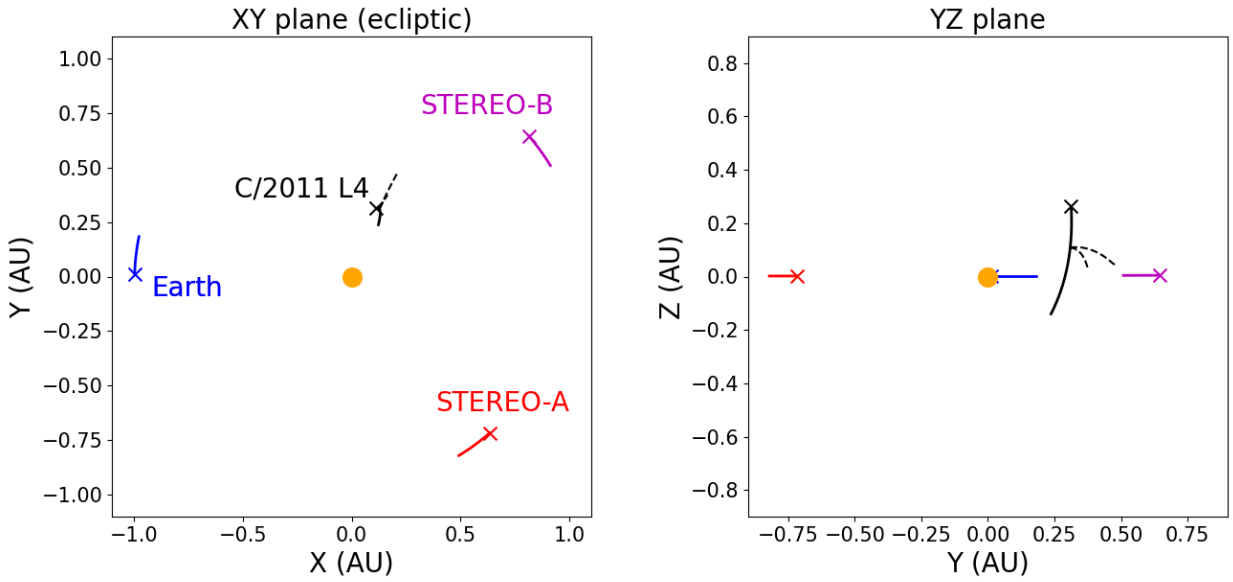

Figure 2: Plots showing the observing geometry of the Earth (blue), STEREO-A (red), STEREO-B (magenta) and C/2011 L4 (black) during the encounter. Orbits are shown from midnight on 2013 March 10, through to midnight on the March 20, at which point the positions of all objects are marked with a cross. The tail orientation is illustrated by a snapshot of its outline at 00:09 UT on March 16. This outline is given the small syndyne with $\beta_r = 0.4$ and the large syndyne with $\beta_r = 3.0$. The coordinate system has X and Y in the plane of the ecliptic, with the X axis out towards the first point of Aries, and north as positive Z.

2.1. STEREO-B

As shown in Figure 2, by 2013 both STEREO spacecraft were roughly three quarters of the way towards superior conjunction with the sun. A complete description of the STEREO SECCHI HI-1 and HI-2 instruments is given by Eyles et al. (2009), with context for observing bright dust tails with these instruments given by Price et al. (2019).

2.1.1. HI-1

Figure 3 shows snapshots of the view of C/2011 L4 from STEREO-B HI-1 (also denoted HI-1B). The camera has a field of view of 20° and central solar offset of 14°, with transmitted images having a pixel scale of 70" pixel^{-1} (Eyles et al., 2009). Whilst observing C/2011 L4, this scale corresponded to a physical resolution of 40 000 to 43 000 km per pixel at the comet's head during the observations. The dust tail extended slightly towards the spacecraft, so this resolution reached as high as 35 000 km in parts of the tail. The imaging cadence was 40 minutes. An animation showing the raw HI-1B dataset can be viewed here:

`https://doi.org/10.5522/04/17081939`

Because observing comets is not the intended function of these instruments, there are several idiosyncracies with the dataset from a cometary perspective. Zodiacal dust contributed to background brightness, and as with McNaught there was overexposure around the comet's coma. Interestingly, the comet was at a very similar distance from the observing STEREO spacecraft as McNaught was during its encounter, and the HI images taken of C/2011 L4 had double the exposure of McNaught. However, the lower activity of C/2011 L4 and its larger perihelion distance meant that the comet was less bright than McNaught. As a consequence CCD bleeding was less severe around the nucleus. Bleeding also occurred from two bright planets. The overexposed Earth around the middle of the images does obscure a small part of the tail, but Mercury did not affect the data.The default FITS headers for the celestial coordinates provided inconsistent results compared with the background star-fields, so the astrometry for the files was recalculated independently using the automated service at *astrometry.net* (Lang et al., 2010).

Although the tail is not as bright or extensive as the apparition of C/2006 P1, there is still plenty of good data for the dust tail of C/2011 L4, and the entire comet remained in the image from 2013 March 10 until late on March 16, with a small data gap of a few hours just before noon on March 12, when the spacecraft rotated and the comet

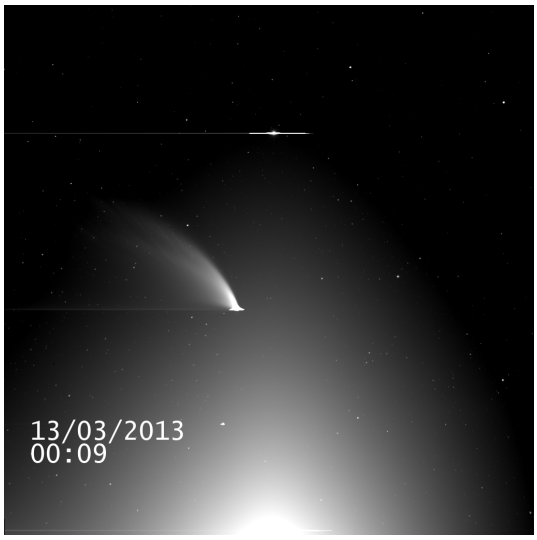

(a) Raw image data

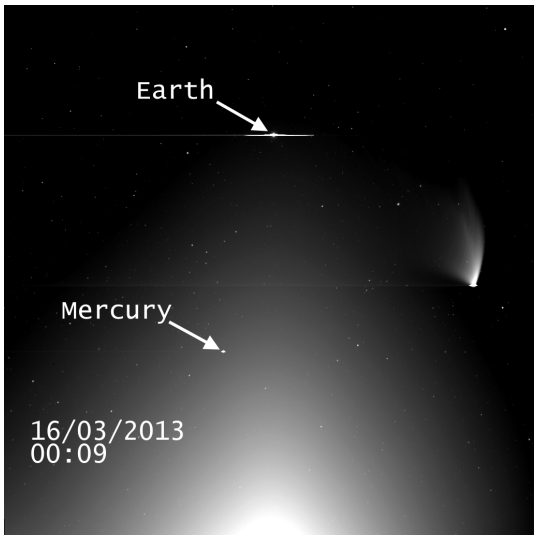

(b) Raw image data

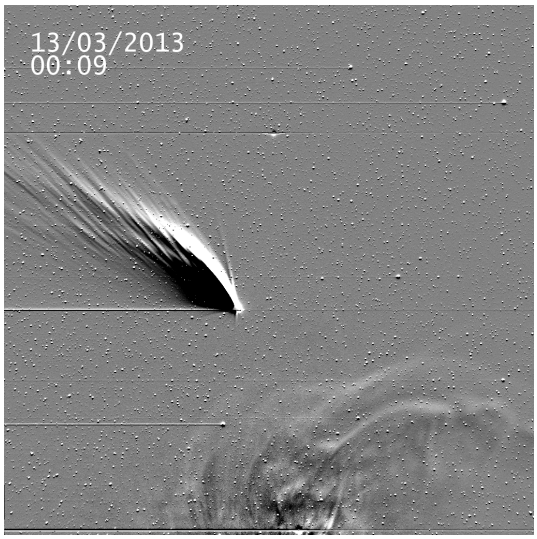

(c) Difference image with wide dynamic range (Coarse Scale)

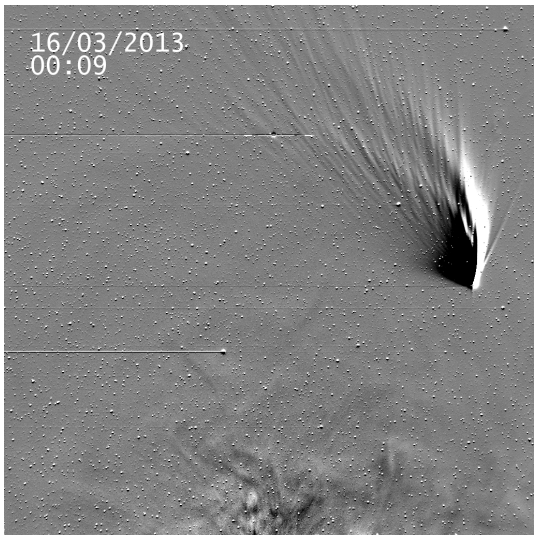

(d) Difference image with wide dynamic range (Coarse Scale)

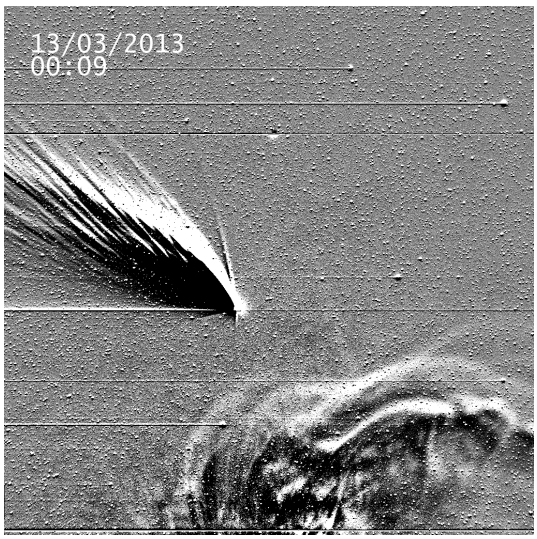

(e) Difference image with narrow dynamic range (Fine Scale)

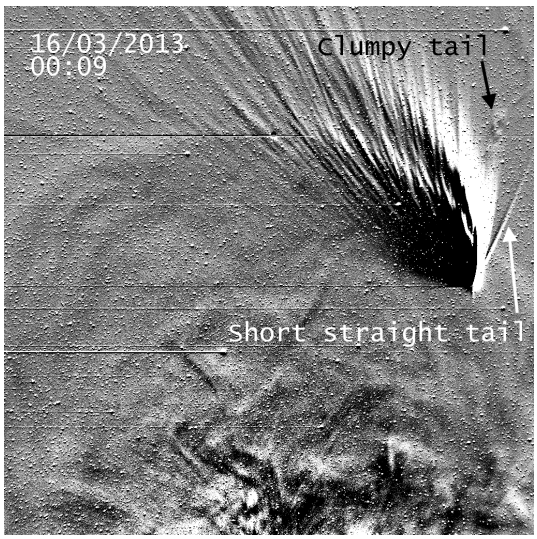

(f) Difference Image with narrow dynamic range (Fine Scale)

Figure 3: Views of C/2011 L4 Pan-STARRS from STEREO-B HI-1. The sun is centre below relative to all images (rotated 90° counter-clockwise and flipped from nominal orientation). The 'clumpy tail' is that studied by Raouafi et al. (2015).

was briefly out of view. There is also some missing data for a small section of the image on March 13 at 08:09. The orbit plane angle was ~-47° at the start of observations on March 10, falling slightly to ~-41° by March 17. This good viewing geometry allowed for the full tail to be clearly observed and provided good conditions for the temporal mapping technique to be applied, described in full by Price et al. (2019).

Unfortunately the Multi-scale Gaussian Normalisation process (Morgan and Druckmüller, 2014) employed by Price et al. (2019) was not particularly successful in enhancing the fine-scale structure in the tail, likely due to the lower signal to noise ratio in this dataset. This analysis therefore makes use of temporal difference images, created by subtracting the preceding image frame from each image. This often reveals fainter fine structure within the image, with the added benefit of 'removing' the largely static F corona. However, while structure is often clearer, intensity values are no longer physical, and bright and dark regions do not necessarily correspond to areas of more or less dust respectively. When inspecting these difference images, it is helpful to display the data with two different brightness scales; one coarse (i.e. with a larger dynamic scale), and one fine, allowing for data in the near-tail and far-tail regions to be studied, respectively.

An animation showing the coarse scale difference image enhanced HI-1B dataset can be viewed here:

`https://doi.org/10.5522/04/17081996`

An animation showing the fine scale difference image enhanced HI-1B dataset can be viewed here:

`https://doi.org/10.5522/04/17082020`

The fine scale difference images in the two bottom panels of Figure 3 most clearly show the other tail phenomena. There is a 'clumpy' tail to the right of the dust tail which is not always clearly visible; this is best seen in the image taken on the 16th. Right of this is another short straight tail. Raouafi et al. (2015) labels these two tails as the HVEC tail and ion tail respectively, whereas Ramanjooloo (2015); Ramanjooloo and Jones (2022) identify them as the ion tail and elemental iron tail respectively. The correct interpretation may be discernable by creating temporal maps of the area surrounding each tail (see section 4.2). Also present in these images is a continuum of dust down to the (type III) dust *trail*, where large dust particles of $\beta_r \sim 0$ lie on the comet's orbit.

The fine scale difference images also show the presence of the interplanetary counterparts of coronal mass ejectae, ICMEs. Whilst it might appear that these ICMEs pass through the comet's tail, the observed sections are most likely to be some distance behind the comet. The HI instrument is designed to image ICMEs through detecting Thomson scattered light; this is most effective around a phase angle of 90°, in the region known as the *Thomson Plateau* (Howard and Deforest, 2012). The phase angle of the comet can be shown to be much higher than this, varying from 122° to 134° (Raouafi et al., 2015).

2.1.2. HI-2

The HI-2 instrument aboard STEREO-B also captured the edge of the extended tail of C/2011 L4. However, as the HI-2B instrument was not in focus, and with only a small part of the tail visible even in difference images, this dataset was disregarded.

2.2. STEREO-A

Only one image of C/2011 L4 was taken by STEREO-A, shown in Figure 4. Whilst the two STEREO spacecraft had deviated from each other significantly by the time of this observation, there was no true stereo image pair of C/2011 L4. By the time the image in Figure 4 had been taken the comet had left the field of view of HI-1B. Furthermore this image cannot be analysed on its own, as the astrometry on the FITS header is not correctly calibrated and the image does not succeed when passed through *astrometry.net*. Some features can be made out by eye, including the two bright syndynic bands of the main tail, the dust *trail* below them, and a very faint tail just above the main tail. However – without the correct astrometry – it is impossible to analyse these features any further; for example, to compare with the HI-1B dataset.

Figure 4: View of C/2011 L4 Pan-STARRS from STEREO-A HI-1. The sun is centre below relative to the images (rotated 90° clockwise from nominal orientation).

2.3. Ground based

The comet reached a peak magnitude of +0.6 on 2013 March 8 a few days before perihelion (Cometary Science Archive, 2021), and was imaged from Earth around this time. In some photographs the comet appeared to display an interesting fine structure with regularly distributed features which appear as synchronic bands. The analysis in Section 5.5 focuses on one such image; Figure 10a, which presents an interesting opportunity for temporal mapping to be applied. This image was taken by Gerald Rhemann using an $f/5.4$ refractor and an exposure time of 240 s.

3. Methodology

3.1. Temporal mapping

We refer the reader to Price et al. (2019) for a full description of the temporal mapping technique. In brief, it provides a new way to visualise the dust tail by moving from a physical projection (e.g. $(RA, dec.)$) to the (t_e, β_r) phase space. In this phase space features are located on the x-axis by t_e; the date and time of their release, and on the y-axis by β_r; their sensitivity to radiation pressure (Equation 1). The assigment of values is based on the production of a Finson-Probstein map of the tail (Finson and Probstein, 1968) through numerical simulation of many dust particles within the tail. Price et al. (2019) demonstrated the temporal mapping method to be robust, consistent, and very useful in constraining the dynamics of the C/2006 P1 dust tail. It proved accurate in keeping features stable within the (t_e, β_r) phase space. This allowed for multiple datasets of C/2006 P1's dust tail to be easily mosaicked, and also eliminated the effects of physical scale, transient motion and observer geometry.

3.2. Other types of temporal maps

Here we introduce a slight variation on the temporal mapping method, used in some of the later plots of this paper. Because each independently parametrised dust particle (t_e, β_r) has its solar system position calculated during the simulation, this three dimensional solar system location (x, y, z) can be transformed to a coordinate system where the xy plane is equivalent to the orbit plane of the comet. Because the 'reduced gravity' force is purely radial, to a good approximation the comet and all its dust exists in this plane, and so in this system all dust has a zero z coordinate. The (x, y) coordinate can then be changed into polar coordinates, giving a unique (R, θ) coordinate for each dust particle. There exists a bijective mapping between these two pairs of coordinates (t_e, β_r) and (R, θ), and it is possible to choose any two of these four coordinates for a working mapping.

Plotting by R is useful when dealing with phenomena where proximity to the sun may be a factor; for example solar wind effects. The units used are astronomical units, where 1 au = $1.495978707 \times 10^{11}$ m. Plotting by θ allows

for features of the same solar longitude; i.e. on the same sunward pointing radial line, to be aligned. The units can be in radians, although the origin point may be arbitrary. A better option is to use the time at which the nucleus of the comet possessed the corresponding value of θ during its orbit. This has the extra benefit of normalising for rarefaction effects that occur as the comet's longitudinal velocity around the sun varies throughout the orbit. For example, the comet's $\frac{d\theta}{dt}$ is highest at perihelion and so an axis using only raw θ values will compress dust features released around perihelion relative to all other dust signatures.

4. C/2011 L4: Temporal mapping results

4.1. Striae in the main tail

As explained in section 2.1.1, the main dust tail of C/2011 L4 seen in the STEREO-B HI-1 data is best visualised using temporal difference images with two different dynamic scales. Two temporal map sequences were thus created:

- A sequence of 235 temporal maps, with fine-scale difference enhancement. This shows the main dust tail from 2013 March 11 00:00 UT until March 18 02:00 UT. Dust is displayed from the region of $0.3 \leq \beta_r \leq 3$ with a wider range of ejection times from 2013 March 01 00:00 UT through to March 13 00:00 UT. Some temporal maps from this sequence can be seen in Figure 5. This sequence is available as an animation here:

  `https://doi.org/10.5522/04/17082035`

- A sequence of 235 temporal maps, with coarse-scale difference enhancement. This shows the main dust tail from 2013 March 11 00:00 UT until March 18 02:00 UT. Dust is displayed from the region of $0.3 \leq \beta_r \leq 3$ with ejection times from 2013 March 05 00:00 UT through to March 11 00:00 UT. Highlighted are two dust points which the analysis later focuses on. Point **P** is highlighted in purple with $\beta_r = 1.7$ and $t_e = 2013{-}03{-}08\ 04:50$. Point **G** is highlighted in green with $\beta_r = 0.8$ and $t_e = 2013-03-05\ 12:00$. Some temporal maps from this sequence can be seen in Figures 6 and 7. This sequence is available as an animation here:

  `https://doi.org/10.5522/04/17082038`

Dust tail structures appear clearly and remain stationary with respect to both apparent time of release t_e and β_r in the temporal maps – as was the case for C/2006 P1 – again indicating the success of the temporal mapping method. Dust generally remained visible for 10-16 days after release from the nucleus, depending on enhancement method used. The maximum observed length of C/2011 L4's tail was calculated as 0.25 AU. This dust was observed on 23:29 on the 17th of March and was 16 days old with characteristic $\beta_r \sim 0.8$.

Similar again to C/2006 P1 is the curved profile of the striae in the temporal mapping projection. This alignment is again taken as confirmation that the striae did not form as near–instantaneous outbursts of dust from the nucleus. Another similarity between the two comets is the bimodal β_r distribution. At C/2011 L4 the two peaks of this distribution appear centred on $\beta_r \sim 0.8$ and ~ 1.8, which is slightly different to the values at C/2006 P1 of $\beta_r \sim 0.7$ and ~ 1.3 (Price et al., 2019).

The fine-scale difference enhancement best highlights the oldest features of the tail, including those older than 10 days which are too faint to be seen using other enhancements techniques. Whilst overexposed closer to the nucleus, dust features older than about 6 to 7 days can be resolved. The coarse-scale difference enhancement provides better detail for the mid-tail where dust is between 5 and 10 days old. This part of the tail is where most of the later analysis is focused, therefore we focus on this dataset for the remaining analysis of the main dust tail.

As mentioned, the instrument astrometric FITS headers proved to be inconsistent and the astrometry for the files was recalculated. Thus, there is unfortunately some anomalous motion within the temporal mapping sequence, which is particularly pronounced for the earliest temporal maps.

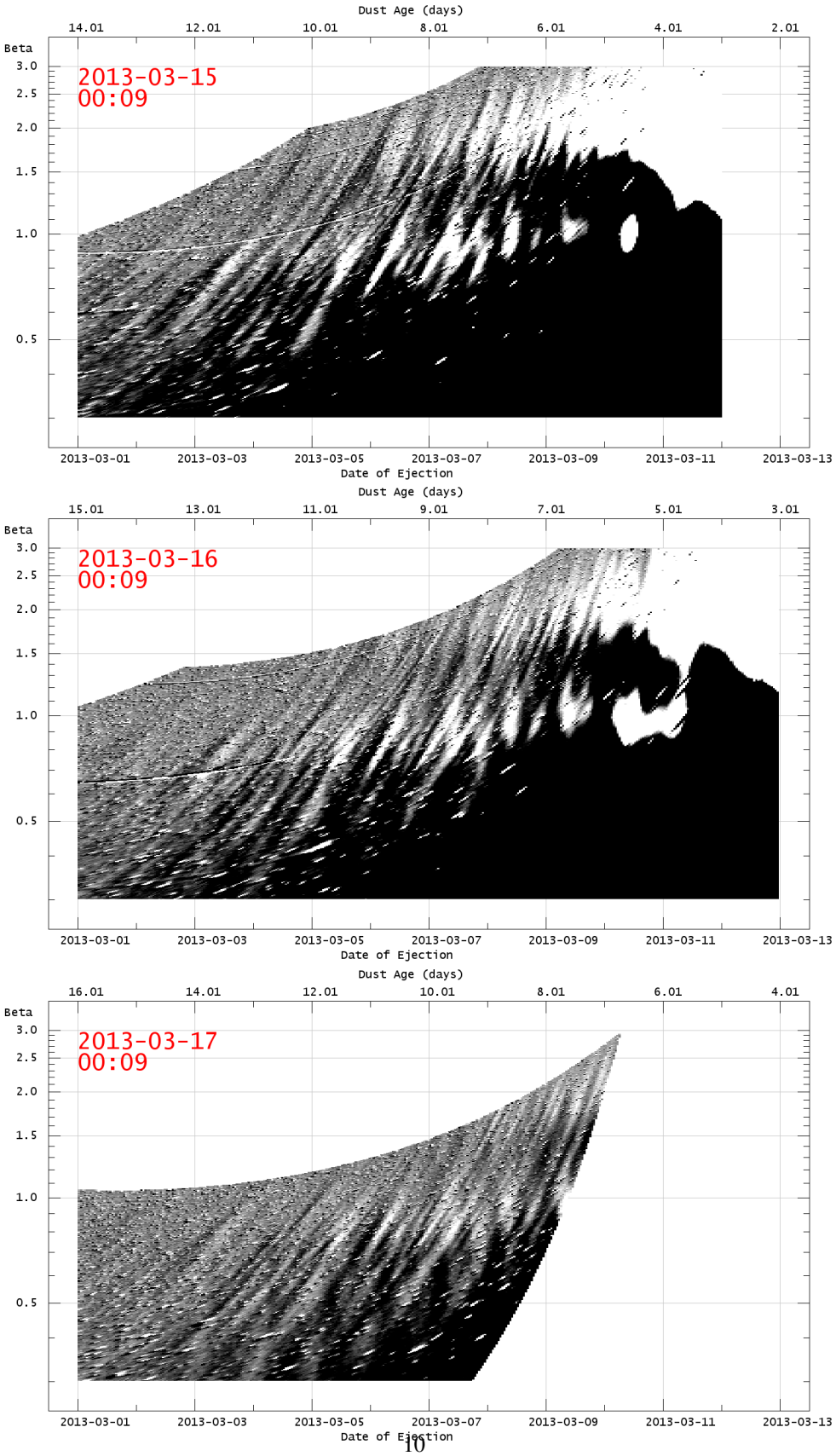

Figure 5: Three temporal maps of the main tail region, based on fine-scale difference enhanced images taken 24 hours apart.

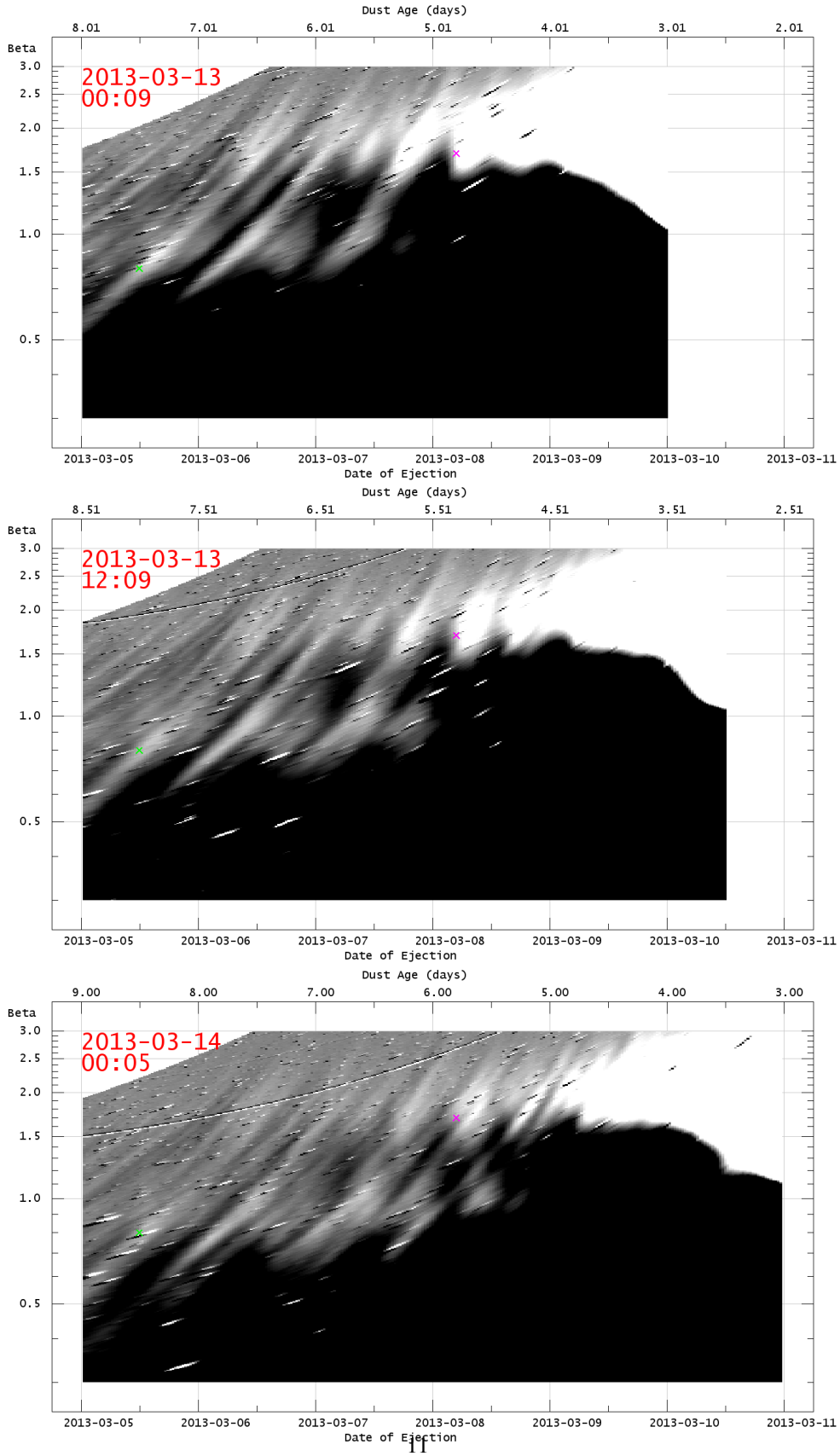

Figure 6: Three temporal maps of the main tail region, based on coarse-scale difference enhanced images taken 12 hours apart. Dust point **P** ($\beta_r = 1.7$ and $t_e = 2013-03-08\ 04:50$) is shown in purple and point **G** ($\beta_r = 0.8$ and $t_e = 2013-03-05\ 12:00$) in green. These two points show areas of clear striae reorganisation.

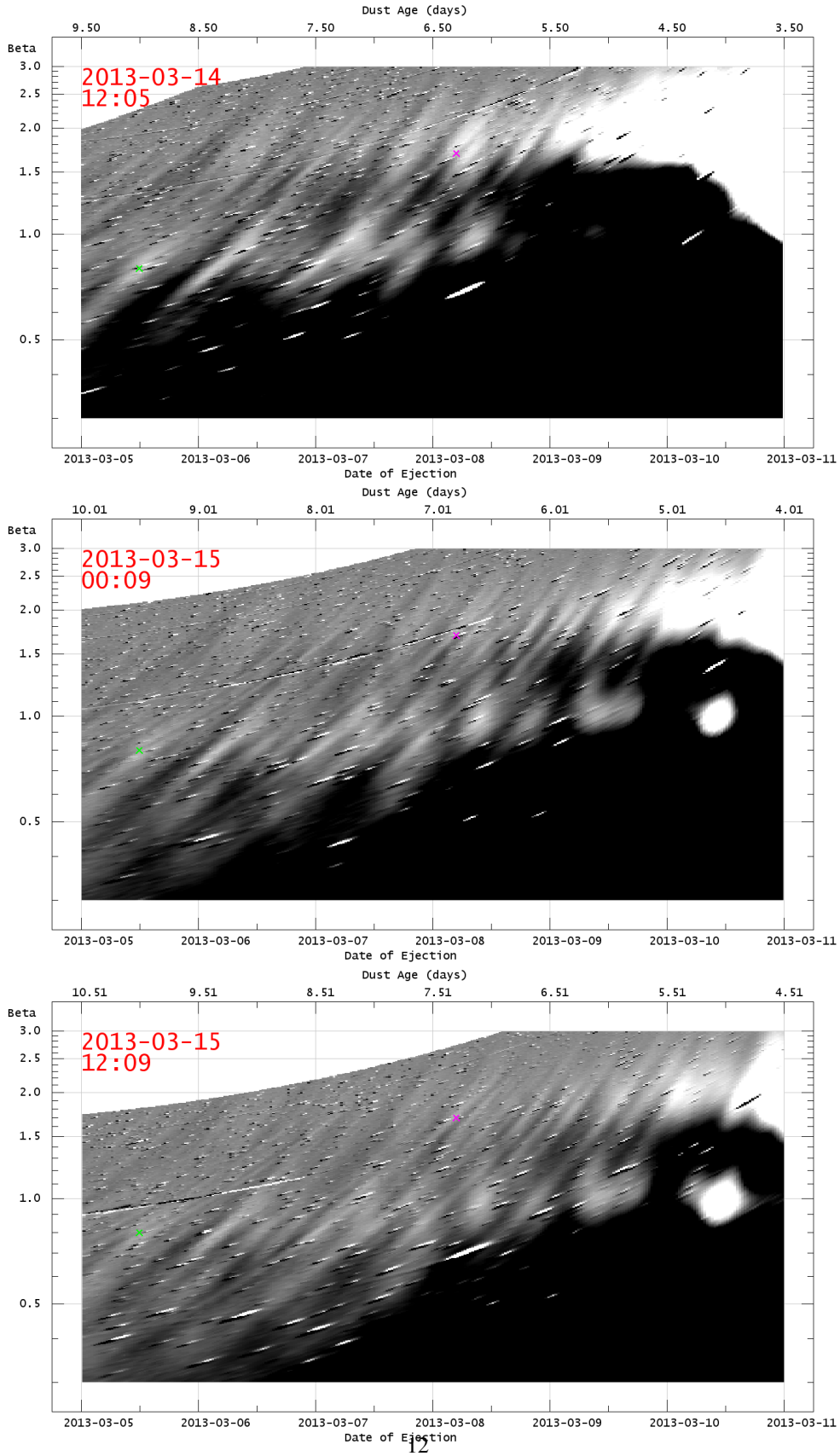

Figure 7: Three temporal maps of the main tail region, based on coarse-scale difference enhanced images taken 12 hours apart. Dust point **P** ($\beta_r = 1.7$ and $t_e = 2013-03-08\ 04:50$) is shown in purple and point **G** ($\beta_r = 0.8$ and $t_e = 2013-03-05\ 12:00$) in green.

4.2. *Clumpy tail region*

In order to help resolve the dilemma between sources that differ on what to label the other tails of C/2011 L4, temporal maps of these two additional tail regions have been created. The *clumpy tail* describes the region given by Raouafi et al. (2015) as the HVEC tail and by Ramanjooloo (2015) and Ramanjooloo and Jones (2022) as the ion tail.

A sequence of 117 temporal maps, with fine-scale difference enhancement was created to study this region. The tail is shown from 2013 March 13 00:00 UT until March 16 12:00 UT. Dust is displayed in the region of $4 \leq \beta_r \leq 20$ with ejection times from 2013 March 11 00:00 UT through to March 14 00:00 UT. This region is not comprehensive in showing this tail as it spans a wide area in the temporal phase space, but it is enough to show the characteristic behaviour of this tail. Two subsections of two temporal maps from this sequence can be seen in Figure 8. This sequence is available as an animation here:

https://doi.org/10.5522/04/17082047

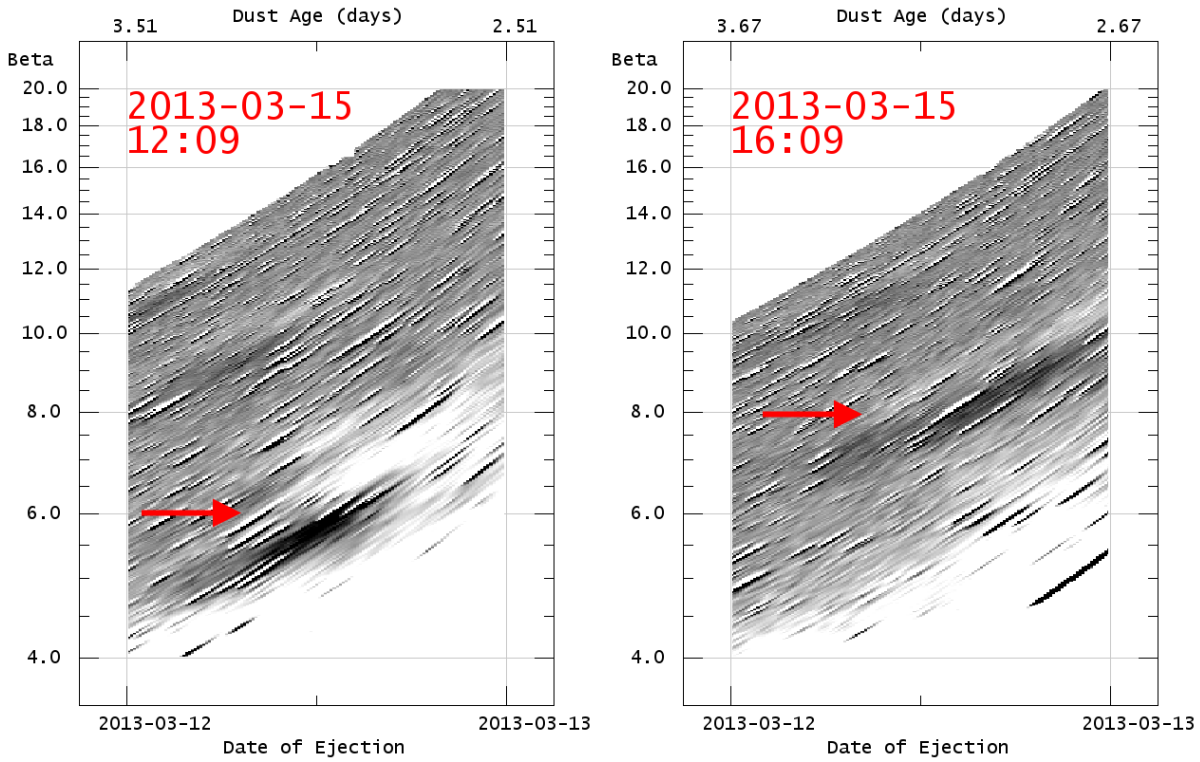

Figure 8: Two temporal maps of the clumpy tail region, based on fine-scale difference images taken 4 hours apart. Labelled with the red arrow, the upwards motion of the feature released after midday on the 12th is common for the features seen in this part of the tail when temporally mapped. Such anomalous motion would appear to rule out Finson-Probstein type physics for this part of the tail.

4.3. *Short straight tail*

The *short straight tail* describes the region interpreted by Raouafi et al. (2015) as the ion tail and by Ramanjooloo (2015) as the neutral iron tail. A sequence of 211 temporal maps, with fine-scale difference enhancement was created to study this region. The tail is shown from 2013 March 10 04:50 UT until March 16 12:00 UT. Dust is displayed in the region of $10 \leq \beta_r \leq 300$. The short extent of this tail means that displaying dust on an axis with fixed ejection time and date proves unsuitable. Dust is therefore shown over a fixed range of ages for each image, i.e. when dust was between 0.1 and 2 days old. As such, the dates and times on the axis are not constant, and fixed points with a specific β_r and t_e move along the axis at the same rate as the cadence of images. A temporal map from this sequence can be seen in Figure 9. The tail can be seen in white and its 'shadow' in black, where it was located in the previous image. This sequence is available as an animation here:

https://doi.org/10.5522/04/17082062

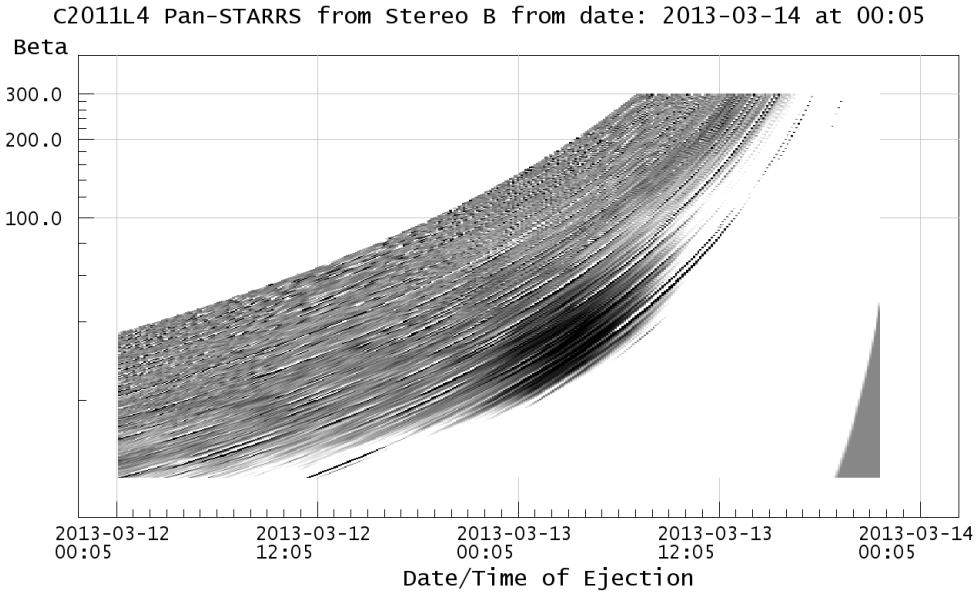

Figure 9: A temporal map of the straight tail region, based on a fine-scale difference image. The tail is shown as the white area above and to the right of its black 'shadow'. The tail generally remains at a high β_r, appearing roughly in the region of $\beta_r \sim 80$ to $\beta_r \sim 120$.

4.4. Ground based data

Using Figure 10a, a temporal map of the comet (on 2013 March 19 as seen from Earth) was created. Because the general brightness gradient of the tail dominates over the fine structure, features in this map are difficult to resolve. Therefore, another version of the temporal map was created by removing the "background" brightness of the tail, shown in Figure 10b. This was achieved by subtracting a Gaussian blurred version of the map from itself.

5. C/2011 L4: Temporal map analysis and discussion

5.1. Striae reorganisation

Given the results of Price et al. (2019), our analysis here concentrates on C/2011 L4 as another case study to investigate striae reorganisation. Compared to the clear reorganisation occurring at C/2006 P1, it is less obvious from the raw STEREO data taken of C/2011 L4's tail that any disruptive processes are happening there. However, there are indications in the fine scale difference images of atypical striae behaviour, with the bottom right panel of Figure 3 shows this behaviour most clearly. In some parts of the tail striae appear "interleaved", with some orientated at a sharper angle intersecting existing features that point closer to the nucleus. At C/2006 P1, this behaviour was characteristic of the reorganisation process and its onset correlated well with the tail's crossing of the HCS. This *interleaved* tail morphology at C/2011 L4 may be indicative that a similar process is happening here.

Any disruptive process happening at C/2011 L4 is certainly more convoluted than what was happening at C/2006 P1, not least due to the decreased brightness and general clarity of the C/2011 L4 data. It is difficult from the HI-1B data to say when the process starts, although it certainly appears to be in progress by the start of the 14th March. Interestingly, the exact morphology of the *disrupted* tail is different from the C/2006 P1 case. Rather than a large number of disrupted features that point sunward mixed with original striae, the tail at C/2011 L4 shows only a few prominent sunward pointing features, which are unevenly spaced. Some pre-existing features appear to stay much more well preserved.

(a) Original Image.

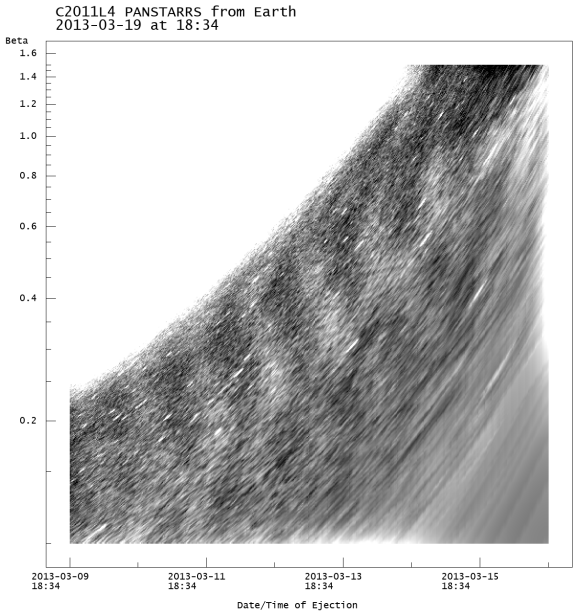

(b) Temporal map with background gradient subtracted

Figure 10: View of C/2011 L4 from Austria, taken on the 2013 March 19, together with an enhanced temporal map. The strong brightness gradient of the tail makes resolving fine structure hard without subtracting the background gradient. This allows the *synchronic band* like features to be seen. Image Credit: Gerald Rhemann.

In order to study the disruption process in more detail at C/2011 L4, analysis is focused on two specific points within the dust tail, which correspond with dust particles arbitrarily chosen from locations where striae disruption is observed:

- Point **P**, which corresponds to a dust particle with $\beta_r = 1.7$ and $t_e = 2013 - 03 - 08\ 04:50$ UT. The evolution of the structure around this dust tail location as seen by STEREO-B HI-1 is shown in Figure 11. Point **P** is labelled with a purple cross in this figure and subsequent figures. An animation showing this dataset can be viewed here:

  `https://doi.org/10.5522/04/17082065`

- Point **G**, which corresponds to a dust particle with $\beta_r = 0.8$ and $t_e = 2013 - 03 - 05\ 12:00$ UT. The evolution of the structure around this dust tail location as seen by STEREO-B HI-1 is shown in Figure 11. Point **G** is labelled with a green cross in this figure and subsequent figures. An animation showing this dataset can be viewed here:

  `https://doi.org/10.5522/04/17082068`

These two dust points provide good examples of parts of the tail which have been disrupted. Both show striae that appear to be split apart during the reorganisation process and end up as "combed" gaps between the original striae fragments, where these gaps have a more sunward facing radial orientation. This behaviour is very similar to what was seen at C/2006 P1. The "combing" process appears to begin between 18:00 UT on the 13th March and midnight on the 14th March for point **P**, and between 12:00 and 18:00 UT on the 14th March for point **G**. Interestingly, the older dust appears to be affected later, as was the case for C/2006 P1. This would appear to rule out reorganisation behaviour being triggered once dust reaches a certain age.

The temporal maps in Figures 6 and 7 show the behaviour of the dust at points **P** and **G** in the radiation beta and ejection time phase space. Largely the maps reinforce what is seen in the raw data; with the new *combed* gaps

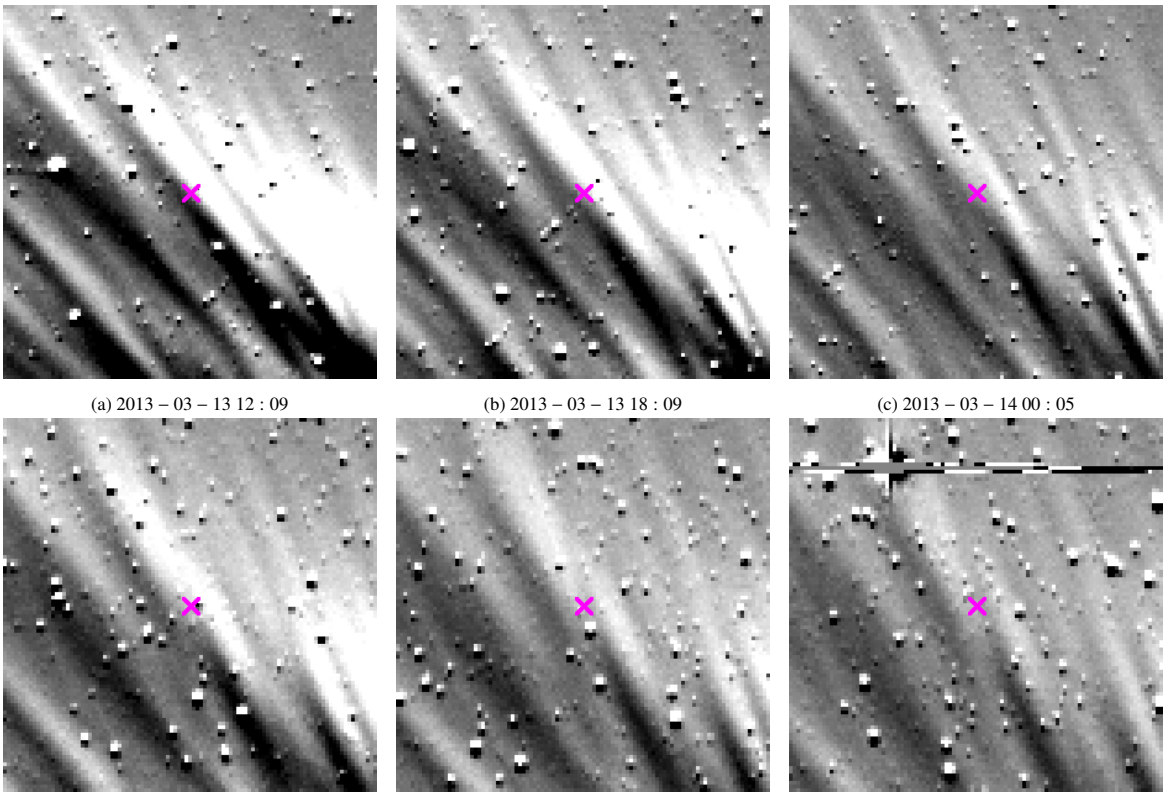

(a) 2013 – 03 – 13 12 : 09 (b) 2013 – 03 – 13 18 : 09 (c) 2013 – 03 – 14 00 : 05

(d) 2013 – 03 – 14 06 : 05 (e) 2013 – 03 – 14 12 : 05 (f) 2013 – 03 – 14 18 : 05

Figure 11: A sequence of images extracted from the STEREO-B HI-1 coarse scale difference images. The breakup of a stria early on the 14th march is shown, centred on the purple point **P** which represents a dust particle with $\beta_r = 1.7$ and $t_e = 2013 - 03 - 08\ 04 : 50$ UT.

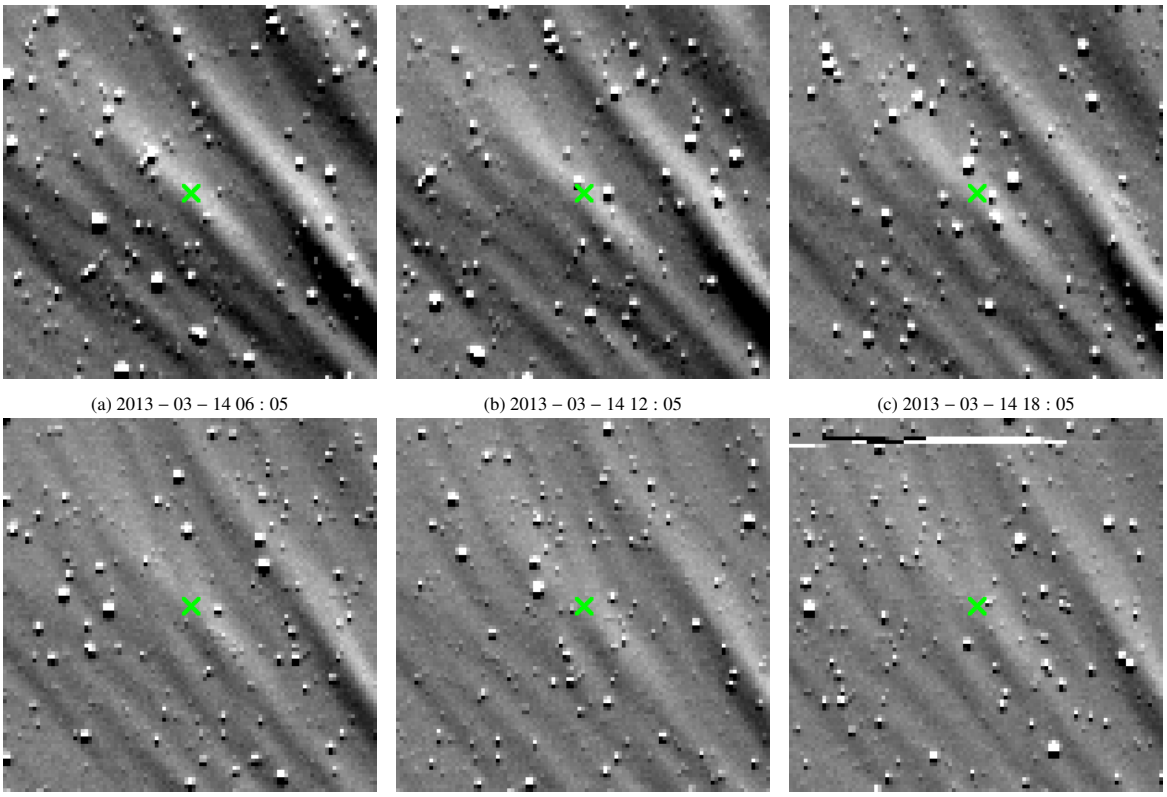

(a) 2013 – 03 – 14 06 : 05 (b) 2013 – 03 – 14 12 : 05 (c) 2013 – 03 – 14 18 : 05

(d) 2013 – 03 – 15 00 : 09 (e) 2013 – 03 – 15 06 : 09 (f) 2013 – 03 – 15 12 : 09

Figure 12: A sequence of images extracted from the STEREO-B HI-1 coarse scale difference images. The breakup of a stria early on the 14th march is shown, centred on the green point **G** which represents a dust particle with $\beta_r = 0.8$ and $t_e = 2013 - 03 - 05\ 12 : 00$ UT.

appearing to intersect original dust at a steeper angle (with respect to the tail's synchrones), and also matches the temporal mapping results from C/2006 P1. One interesting result at C/2011 L4 is the discrepancy for the feature at point **P**. At 12:09 on March 13th, it appears in the raw HI-1 data as a single striated feature. In the temporal map of this image, the stria already seems to be composed of two distinct features. It is perhaps the case that two separate striae already existed but were too close in ejection time to be seen distinctly in the original dataset.

The hypothesis for the C/2006 P1 event presented by Price et al. (2019) was that the Lorentz force causes disruptions to the tail as it crosses the Heliospheric Current Sheet. This second observable case provides a good test of whether this explanation might explain the *general* case of striae disruption.

5.2. Evidence for Solar wind effects

To study the solar wind conditions at C/2011 L4, the CORHEL heliospheric model was used. For full details, please refer to Price et al. (2019). This model was used to generate solar wind conditions for Carrington Rotation (CR) 2134 (2013 February 22 to March 21). This model employs solar magnetogram data from SOLIS (Synoptic Optical Long-term Investigations of the Sun) provided by the National Solar Observatory.

Like C/2006 P1, C/2011 L4 is also a comet with a high orbital inclination. It was within the ±60° heliolatitude simulation domain between 2013 March 5th until the end of CR 2134 on March 21st. C/2011 L4 entered the simulation domain at around 0.337 AU (72.5 solar radii), reached perihelion at 0.302 AU (65 solar radii) on March 10th at 04:05 UT. It then crossed the HCS twice, first on the 12th at around 05:00, and then again on the 13th at 17:30. The comet generally remained in a region of slow solar wind until the 15th. By the end of CR 2134 it was at a distance of 0.454 AU (98 solar radii).

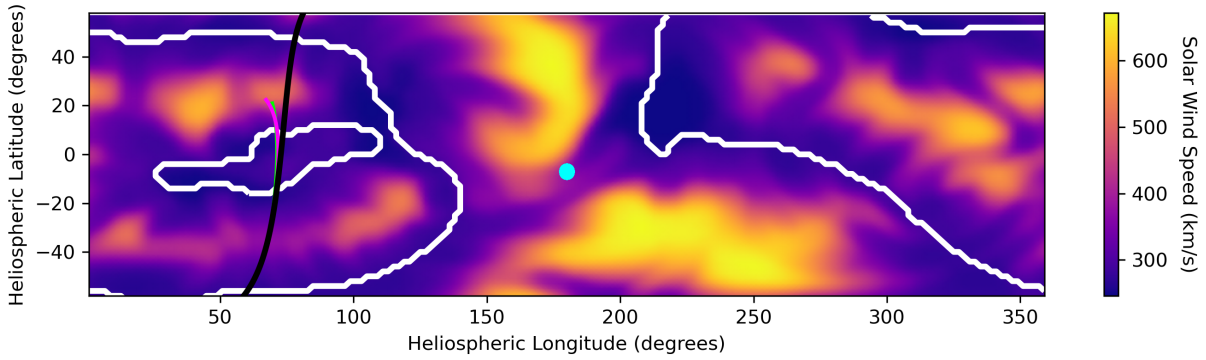

Figure 13: A Mercator projection map of CORHEL modelled solar wind speeds for the 12th March 2013, Carrington rotation 2052, at a distance of 0.304 solar radii (SOLIS data). The coordinate system is Stonyhurst heliographic, rotated by 180° around the Z-axis. The HCS is traced by the white line. C/2011 L4's track is the inclined black line; motion was from south to north. The track of dust point **G** is shown in Green, and the track of dust point **P** is shown in purple, both south to north. Dust at both points is shown for 16 days. The sub-Earth position is shown in cyan. Note that the actual conditions are only roughly shown in this map as the comet varied heliospheric distance, and the simulation evolves with time.

The CORHEL results for solar wind conditions at the nucleus of C/2011 L4 are shown by the black lines in Figures 13 and 14. The results based on SOLIS data imply a complicated picture for the comet whilst in the STEREO-B HI-1 field of view (March 10 to 16), where C/2011 L4 crossed the HCS sheet twice (March 12 & 13). The first crossing occurred whilst in the southern hemisphere, from inward magnetic polarity to outward polarity. The second crossing took place after the comet had moved into the northern heliosphere, as the magnetic polarity changed back from outward to inward. Unlike the C/2006 P1 crossing, the rest of the solar wind conditions were less volatile, staying roughly constant until the 15th.

This second case of a clear correlation between the obvious changes in the striae orientation and the crossing(s) of the HCS reinforces the case for an interaction between the solar wind and comet. As explain by Price et al. (2019), this would occur through the change in the direction of the Lorentz force associated with the change of direction of the heliospheric magnetic field associated with a HCS crossing. Such an observable effect was predicted by Horanyi and

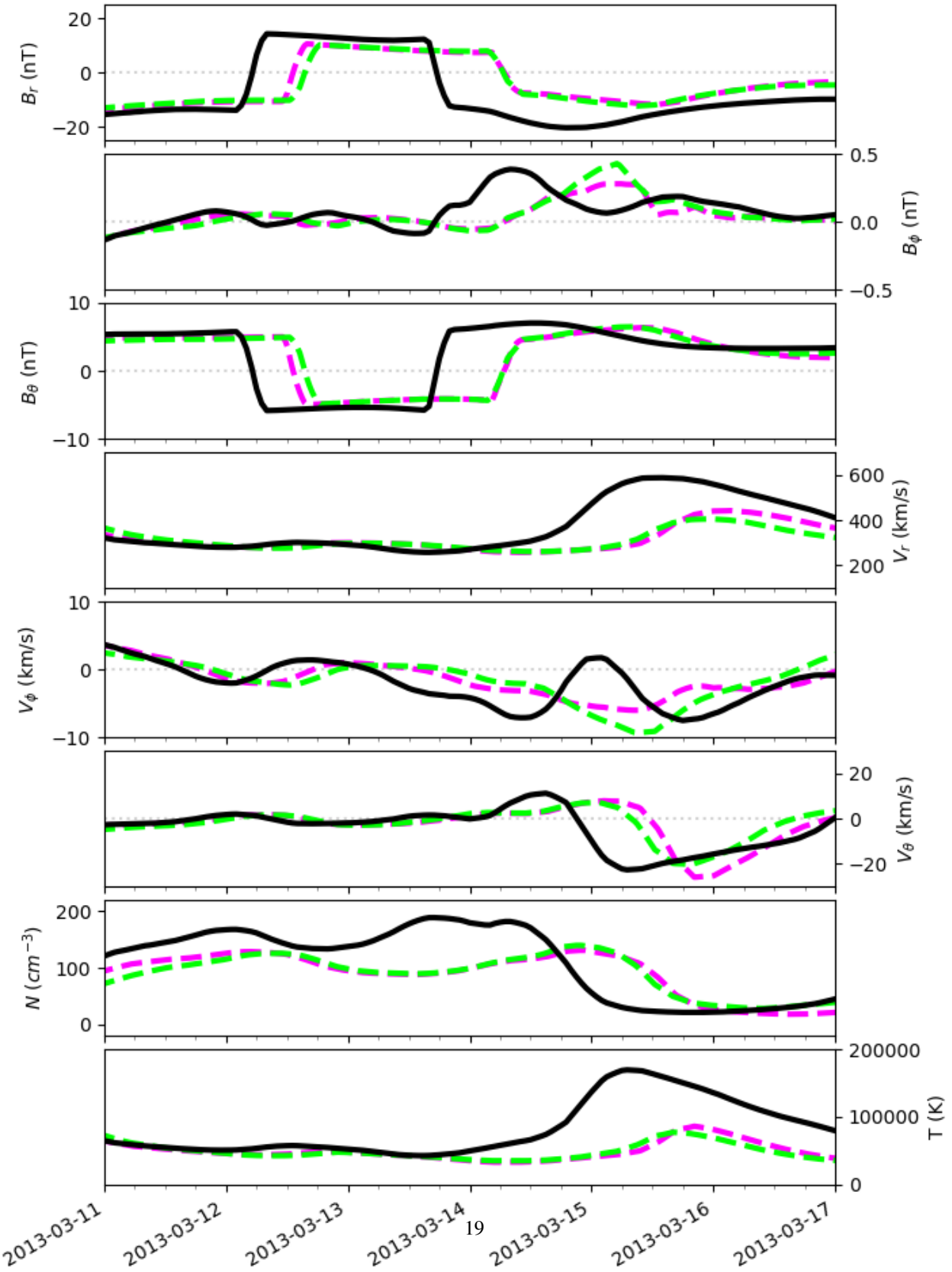

Figure 14: Solar wind conditions at C/2011 L4 estimated using the CORHEL model with SOLIS data. The properties have been extracted along the path of the nucleus of C/2011 L4, shown in black, as well as along the paths of dust points **P** and **G**, shown in purple and green respectively. From top to bottom, the panels show the three components of the heliospheric magnetic field in the Stonyhurst heliographic coordinate system; three components of the solar wind speed in the same system, the solar wind particle number density, and finally the plasma temperature.

Mendis (1987), and described more recently by Mendis and Horányi (2013), with Kramer et al. (2014) also finding that the Lorentz force plays a role in influencing tail morphology at high heliocentric distances.

The potential strength of the Lorentz force can be estimated by the following equation (Kramer et al., 2014; Price et al., 2019):

$$a_{Lorentz} = \frac{12\varepsilon_0 V}{C^2}\beta_r^2 \frac{\rho_d}{Q_{pr}^2} B_\phi v_{sw} \tag{2}$$

The solar wind conditions at C/2011 L4 differed from those at C/2006 P1, particularly as this event took place slightly further from the sun. Figure 14 gives conservative values as $B_\phi = 5$ nT and $v_{sw} = 250$ km s^{-1}. Dust is again assumed to be positively charged to around +5 V (Gustafson, 1994). This gives:

$$a_{Lorentz} = \beta_r^2\, 0.0021 \text{ m s}^{-2} \tag{3}$$

However, the Finson-Probstein acceleration a_{FP} is smaller as well due to the increased heliospheric distance, though not affecting grains' β_r value due to parallel fall-off in solar gravitational pull and photon flux. At $r = 0.308$ AU, where the first crossing occurred:

$$a_{FP} = \frac{(1-\beta_r)GM_\odot}{r^2} \approx (1-\beta_r)\, 0.06 \text{ m s}^{-2} \tag{4}$$

With the assumption of a continuous Lorentz force acting on the dust before the HCS crossing, there would be a change of B_ϕ from 5 nT to -5 nT. Hence the change of the Lorentz force may account for a sudden perturbation in the motion of the dust in this case up to about 7% the magnitude of gravity and radiation pressure, and higher for high β_r dust. This should still easily be enough to affect the dynamics of the tail.

As with C/2006 P1, the estimated solar wind conditions that can be easily derived are accurate for the comet's head only. For the rest of the dust tail, the HCS crossing time will also be different from the *unperturbed* CORHEL model as the magnetic field drapes around the comet's head. Dust particles in the coma in particular will therefore have likely encountered a complex magnetic field structure, not a relatively simple reversal of magnetic field direction, though clear of the coma and ion tail, solar wind conditions would be expected to closely resemble the unperturbed values. In addition, due to the rotation of the sun and rest of the HMF, the exact locations in inertial space where the Lorentz force is affecting the tail was almost certainly changing with time.

The CORHEL model should still give a reasonable approximation of what the conditions were like in the tail, and this can account for the rotation of the HMF and HCS positions. Using the CORHEL model, the solar wind conditions at the two dust points **P** and **G** can be estimated. These results are shown in figures 13 and 14 by the purple and green lines for points **P** and **G** respectively. The predicted times of all HCS crossings are shown in Table 1, alongside the observed times of striae disruption as seen in the STEREO-B HI-1 images.

	Simulated		Observed
	Inward to Outward	Outward to Inward	
C/2011 L4 Nucleus	12th 05:00	13th 17:30	-
Point **P**	12th 13:00	14th 06:45	13th to 14th 18:00 to 00:00
Point **G**	12th 15:30	14th 06:30	14th 12:00 to 18:00

Table 1: Comparison of CORHEL simulated HCS crossing times and observed striae disruption times. All times are in UT and dates from March 2013. Note that simulated times are only rough estimates, particularly for dust in the tail; this region of space will be affected from the interaction of the HMF with the comet and the formation of the ion tail.

These results show some agreement between the observations and the simulations. The simulated second crossings of the HCS from outward to inward magnetic polarity for both dust points **P** and **G** are both within twelve hours of the onset of observed striae disruption. Given the limitations of the simulation, this rough agreement would seem to add to the evidence that the reorganisation process is linked to the solar wind's properties. The 'original' stria at point

P also appeared to consist of two closely overlapping but distinct striae when studied within the temporal maps. This separation may have been caused by an earlier reorganisation process from the first HCS crossing, before the striae were disrupted fully by the second HCS crossing.

In section 4.1 it was also seen that the reorganisation process at C/2011 L4 appeared to be more complex than the C/2006 P1 case. In particular there was more inconsistency with which striae were affected. This may be due to the more complex nature of this event as there were two HCS crossings, but also the relative weakness of the Lorentz force compared with the C/2006 P1 event. More generally, the interpretation of striae means that there could be at least six "families" of dust grains present in the tail:

1. released prior to either HCS crossing, which did not later cross the HCS during the observation period, and remained unperturbed by any change in the motional electric field.
2. released prior to the first HCS crossing, which subsequently crossed the HCS once, during which time their dynamical behaviour was altered, but did not cross a second time.
3. released prior to the first HCS crossing, which crossed the HCS twice, each time at which their dynamical behaviour can be assumed to have been altered.
4. released after the first HCS crossing, which did not later cross the HCS a second time and so did not experience any dynamical behaviour change.
5. released after the first HCS crossing, which subsequently crossed the HCS at the second crossing, during which time their dynamical behaviour was altered.
6. released after the second HCS crossing, in a "new" near-steady magnetic field regime, which was unaffected by changes during either HCS crossing.

The complexity of this event would make it extremely difficult to fully analyse and constrain the behaviour of the dust. This is even without considering the unresolved and ill-posed problem of striae formation. To ascertain further information, the alignment of the reorganised or 'combed' striae is instead considered later, in Section 6.

5.3. HVEC tail or ion tail?

Figure 8 shows two temporal maps of the *clumpy* tail region. The tail clumps appear to move vertically upwards in the temporal maps over time, although they do generally stay at the same horizontal location. This motion within the temporal maps is unlike any dust features that have been so far mapped, even including high β_r tails such as the iron tail of C/2006 P1. This anomalous motion would appear to rule out Finson-Probstein type physics for this part of the tail.

This result rules out a possible explanation of the tail as a high β_r tail of neutral atoms. As for the other possibility of the tail as a charged dust phenomenon given by Raouafi et al. (2015), it can be noted that their assumed magnetic field of 30 nT is larger than the value found from the CORHEL simulation. Additionally, the given speeds of 600 km s^{-1} to which particles are supposedly accelerated is far larger than the values for the solar wind speed given around the comet from this model. The interpretation of the clumpy tail as an ion tail given by Ramanjooloo (2015) and Ramanjooloo and Jones (2022) was used to derive solar wind speeds that lay between 200 and 400 km s^{-1}, which is much more in agreement with the CORHEL simulated results. Before a conclusion can be drawn on the most likely interpretation, the orientation of the short straight tail must also be considered, as the interpretation of both tails depends somewhat on each other; they of course cannot both be ion tails.

5.4. Ion tail or elemental tail?

Figure 9 shows a temporal map of the *short straight tail*. The tail (and its difference image caused 'shadow') appears in the very high β_r region in the temporal maps, and if it is interpreted as being a Finson-Probstein type phenomenon, its lifetime would also appear to be very short. There are no features that can be tracked with respect to a specific emission time. However, its temporal extent as a F-P feature also stays constant, generally lasting about 16-18 hours. It is slightly less consistent in its position with respect to β_r. Whilst it does roughly stay in the same area in these high β_r maps, there is quite a large variation in the position of the tail's largest extent, with the "peak" of the tail varying between $\beta_r \sim 80$ to $\beta_r \sim 120$. However, the compression of high β_r syndynes in physical space means their mapping is extremely sensitive to variations in the astrometry of the image, which is already known to be a problem (see section 2.1.1 for details). The potential for a neutral tail to exist at a high $\beta_r \sim 80$ is of course

possible, such a sodium tail was the first elemental tail reported by Cremonese et al. (1997), with a characteristic $\beta_r = 82 \pm 3$. Additionally, there is no reason why an ion tail would remain at such a fixed position within the temporal maps, especially when the solar wind velocity was known to be varying.

From all the evidence in the temporal maps of both the clumpy tail and short straight tail, and the CORHEL simulation results, the conclusion by Ramanjooloo (2015); Ramanjooloo and Jones (2022) by far seems the most probable. This interpretation gives the clumpy tail as a disparate ion tail, with the short straight tail appearing to be some kind of elemental tail. The high β_r, incompatible with neutral Fe emission observed by the same instrument for C/2006 P1 (Fulle et al., 2007) indicates that this is likely a neutral sodium tail. We note that the HI-1 effective bandpass is only a few percent at the wavelength of the Na double D line (Bewsher et al., 2010; Jones et al., 2018), implying that C/2011 L4's sodium tail was considerably brighter than that of C/2006 P1 and/or that the HI-1 bandpass had altered between the C/2006 P1 observations in 2007 and these made in 2013.

5.5. Ground based data

Figure 10b shows a ground based image of C/2011 L4, and an enhanced version of its temporal map. This temporal map is very different from any of those generated from STEREO-B data. The faint dust features have an alignment more suggestive of synchronic bands rather than of striae, appearing more vertical than any features seen by HI-1B. They also extend over a different range of β_r, roughly in the region of $0.2 \leq \beta_r \leq 1$, as opposed to dust seen from STEREO-B which had $0.3 \leq \beta_r \leq 3$. Although it was taken some time after the STEREO images, there is a small overlap of Figure 10b – which mostly shows dust features formed after perihelion – with the bottom right of 5, although it is difficult to match up any features between the two maps.

This result is quite curious. It provides the first test of temporal mapping from two very different observer geometries, with STEREO-B being roughly three quarters of the way towards superior conjunction with the sun relative to Earth. The vast difference between the two temporal maps is a reflection of the difference in the appearance of the comet from the two observers (see Figure 3 and Figure 10a). This could be caused by a number of factors. Instrument design including bandpass may be one cause. Additionally, whilst the viewing geometry should be removed on a basic level by the temporal mapping, differences in the phase angle of the dust throughout the tail may cause different parts of the tail to be more or less bright dependent on observer position, as a consequence of the dust phase function. Temporal mapping does not correct for such differences. The potential to learn more about C/2011 L4 from ground based data is complicated by these factors and has been deemed to be beyond the scope of this work.

6. C/2011 L4 and C/2006 P1: Alignment of combed striae

So far, the analyses here and in Price et al. (2019) on the striae reorganisation processes at C/2006 P1 and C/2011 L4 has concentrated on the temporal links between the processes and the behaviour of the local solar wind conditions. The spatial component of these reorganisations is now considered. At each comet, new striae-like features formed after each reorganisation, appearing as new continuous features which span the dust tail, like those seen in Figure 1. These *combed* features cross the original striated tail and appear to point roughly sunward.

Whilst an obvious explanation might be that these new features form simply the same way as the original striae, there are complications for this interpretation. Such fragmentation models (summarized in Section 1.2) work because the relatively short distances over which fragmented clouds of dust spread out are magnified when the dust diffuses out into the full tail. At C/2006 P1 for example, new combed features appear to spread across a tail that is already a significant fraction of AU in size. Hence, the structure of these features must be created in some other way. Here, the orientation of these features and its implications for their structure is considered.

6.1. Are the features sunward aligned?

From a brief visual inspection combed features appear to point sunward. This is a good place to start the analysis, as the mapping process to a sunward aligned coordinate system is fairly trivial. As was explained in section 3.2, there exists a bijective mapping for each dust particle from the (β_r, t_e) phase space to the position (R, θ) in the orbital plane. Additionally, any two parameters form a non-degenerate phase space for which to replot the dust tail.

For the purposes of the analysis here, the parameter space (β_r, θ) was chosen as this provides the best visualisation of the sunward alignment of features. The HI-1A dataset for C/2006 P1 with Multi-scale Gaussian Normalisation

(MGN) enhancement (see Morgan and Druckmüller (2014); Price et al. (2019) for details) and the HI-1B Coarse-scale difference enhanced dataset for C/2011 L4 were replotted in this phase space, shown in figures 15 and 16 respectively. The θ axis is not denoted by radians but instead by the date and time at which the nucleus of the comet possessed the corresponding θ; equivalent to the time the nucleus was associated with that particular sunward direction. Because comets have highly eccentric orbits, this avoids rarefaction effects along the θ axis as the longitudinal velocity of the comet is highly variable around perihelion. An animation showing the sunward aligned temporal map sequence seen in Figure 15 can be viewed here:

`https://doi.org/10.5522/04/17082149`

An animation showing the sunward aligned temporal map sequence seen in Figure 16 can be viewed here:

`https://doi.org/10.5522/04/17082158`

These initial results show that features at both comets do not present as purely sunward aligned features once they are visible. Features at C/2006 P1 appear to be closer to this orientation than those at C/2011 L4, which appear to differ more from the radial case.

Interestingly, this (β_r, θ) mapping proves to provide the clearest visualisation of the reorganisation process. In Price et al. (2019), it was reported that there was some difficulty in identifying the onset of the reorganisation process at C/2006 P1, with the earliest definite observations occurring on January 13th 2007. Figure 15 shows that reorganised features first became visible in the first image taken after the six hour data gap ending at 22:01 on January 12th. Furthermore, the reorganisation process appeared to affect the oldest dust first, the youngest dust second, with some parts of the mid tail being the last to experience the combing. This appears to indicate the extremely spatially localised nature of the disruption, as might be expected due to the relative motions of a warped HCS and the dust tail. The spatial nature of the reorganisation at C/2011 L4 is much harder to resolve; the difference images do not give such a clear view of the combing, and other enhancements (e.g. MGN) are too noisy to see any of the tail structure.

Although these mappings do not show the features to have formed with a sunward alignment, it is not so simple to rule out that a sunward orientation never occurs, because the orientation of features will constantly become increasingly tilted within this mapping due to the nature of the Finson-Probstein motion. If the features formed from some initial process with a sunward alignment, after which dust took several hours to be reorganised into a visible feature, this off-radial explanation might be expected from newly appearing features. Therefore in order to fully characterise a possible sunward explanation, the previous 'theoretical' alignment of newly formed features must be considered.

The (β_r, θ) locations of the striae can be traced backwards within the data by tracking the relevant dust by its corresponding (β_r, t_e). This shows how features would have been aligned before they have formed. This gives a non-visible timescale for combed feature formation; the time between the theoretical sunward alignment and actual manifestation of observed dust features. This tracking is applied to a selection of combed features that had clearly formed by the last panels of Figures 15 and 16. The formation timescale can then be estimated by the time elapsed since a fully sunward alignment of these features; this process is shown in Figures 17 and 18.

The derived formation timescales for the features at both comets appear to differ somewhat. At C/2006 P1, combed features appear much steeper in the (β_r, θ) phase space, and this corresponds to origins as purely sunward features 8 to 14 hours previously. At C/2011 L4, because combed features appear less radially aligned than at C/2006 P1, their previous theoretical sunward alignments occur after a much larger delay of 1 to 3 days. There is more uncertainty to this timescale for C/2011 L4 however, as it harder to pinpoint an exact appearance time for each feature. Even with conservative estimates, there are definitely features that would have taken 2 days to appear within the maps from a sunward alignment. For example, the dust point **G**, marked in green in figures 16 and 18, corresponds to a feature that at the earliest was resolvable around midday on the 2013 March 14. Such a feature corresponds only to sunward alignment around midday on March 12.

An interpretation of whether these results seem plausible is somewhat dependent on the timescales on which the reorganisation process occurs, including the time before which the process can be visually confirmed. These are all still unknowns. The CORHEL simulations are not reliable enough to construct a distinct timeline accurate to less than a few days between HCS crossing and reorganisation event for any part of a dust tail. The visual reorganisation process also appears to vary in the time taken. Combing of striae may occur with the same broad physical explanation but could differ greatly on specific details; C/2006 P1 and C/2011 L4 encountered different solar wind conditions at differing heliospheric distance and stages of the solar cycle.

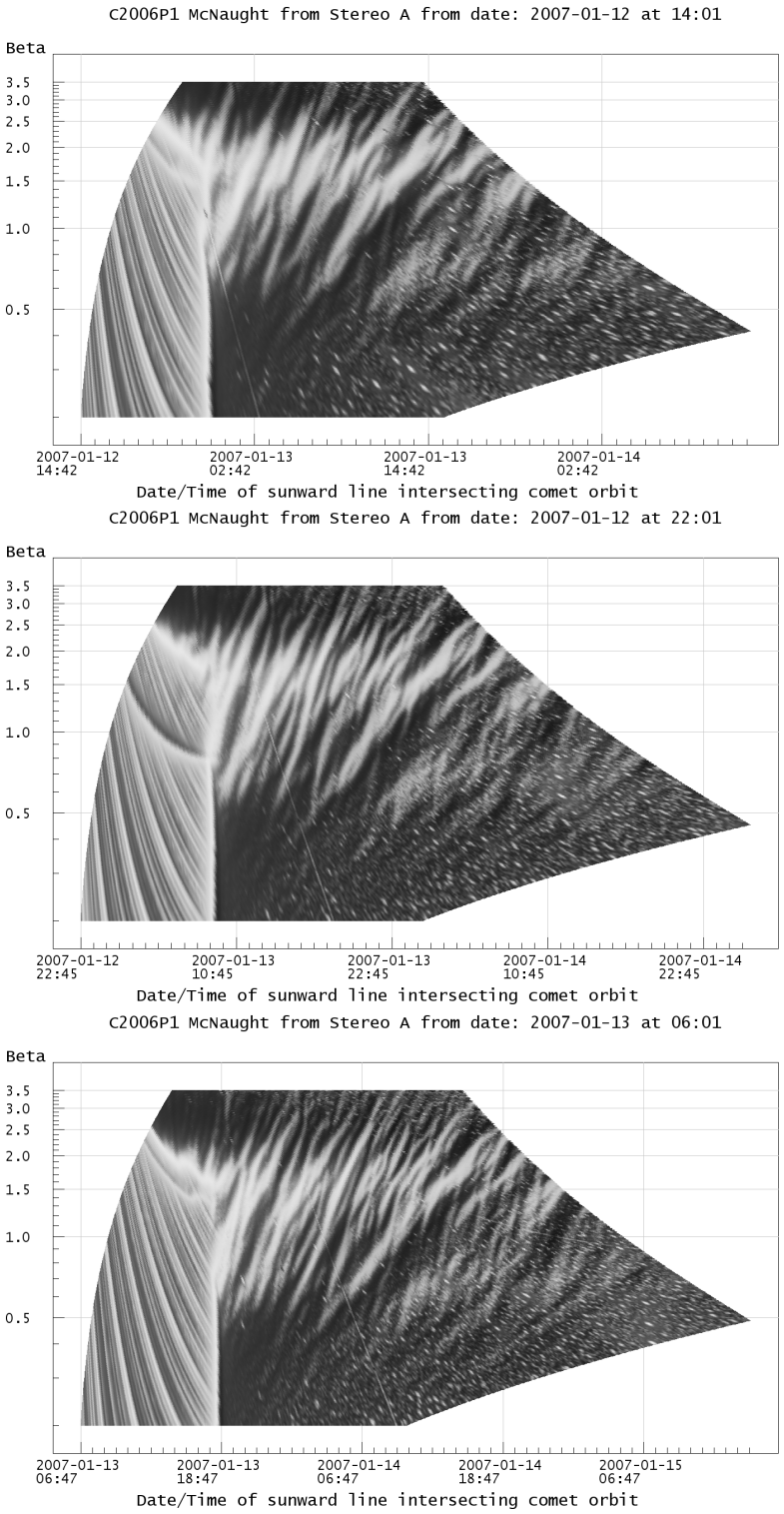

Figure 15: Three sunward-aligned temporal maps of C/2006 P1's main dust tail region as seen by HI-1A with MGN enhancement, taken 8 hours apart. After a 6 hour data gap, on 22:01 on January 12th 2007, new near vertical *combed* features are visible which intersect older striae. Note that features on the far left of the temporal maps are artefacts from the overexposed region near the comet's nucleus.

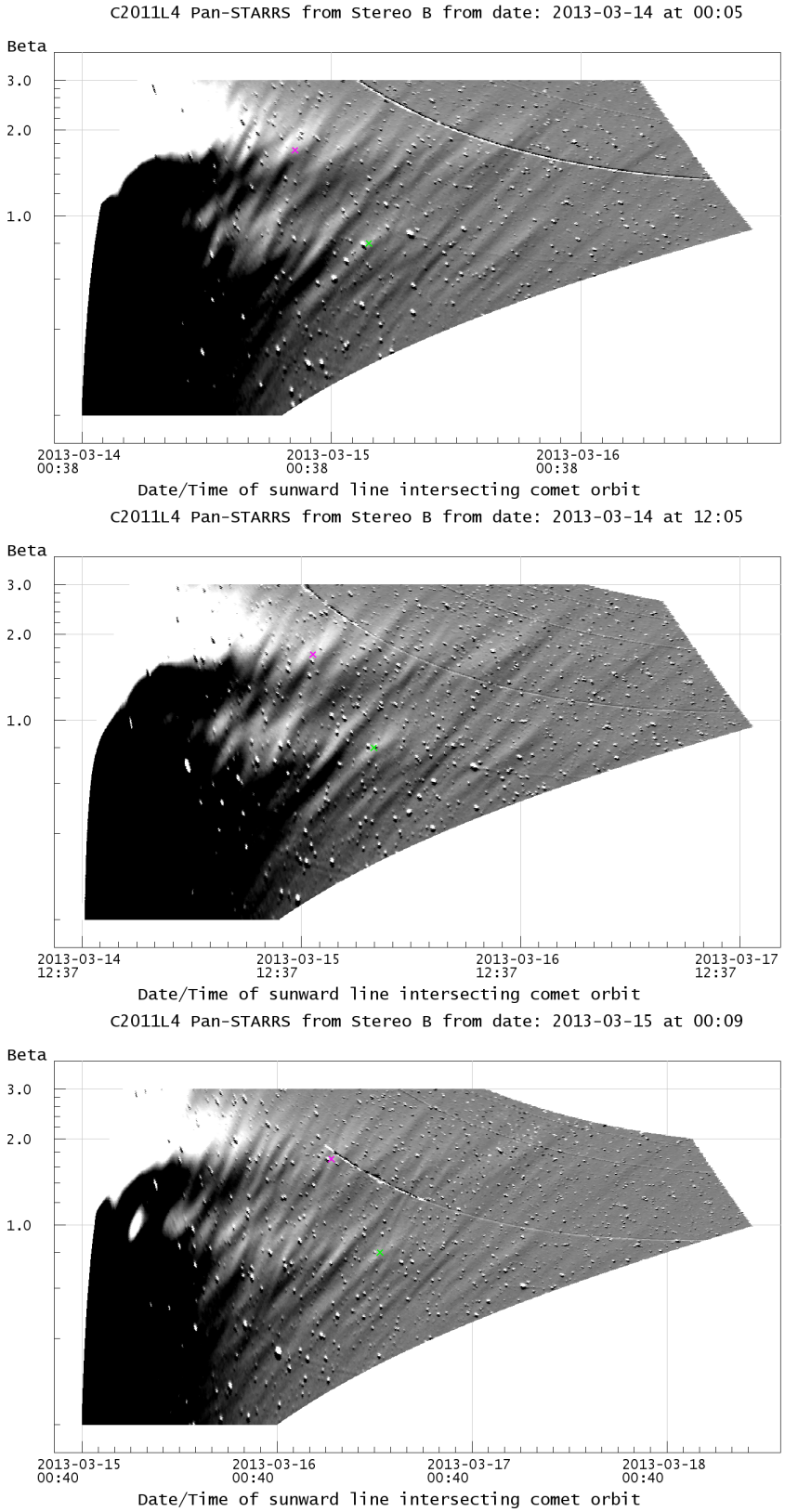

Figure 16: Three sunward-aligned temporal maps of C/2011 L4's main dust tail region as seen by HI-1B with coarse-scale difference enhancement, taken 12 hours apart. A new combed stria feature appeared to form at dust point **G** ($\beta_r = 0.8$ and $t_e = 2013-03-05\ 12:00$) over the course of 14th March 2013.

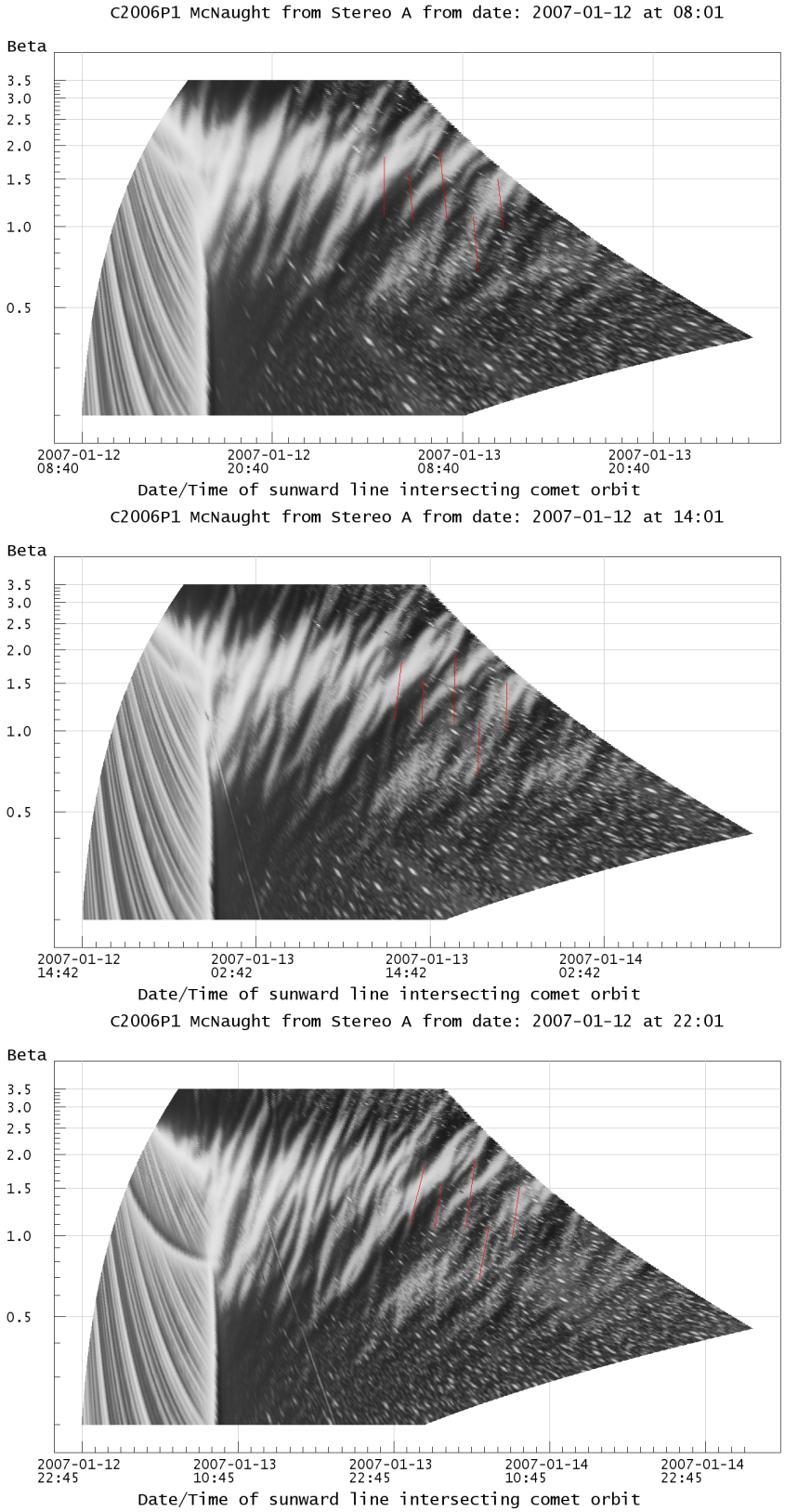

Figure 17: Three sunward-aligned temporal maps of C/2006 P1's main dust tail region as seen by HI-1A with MGN enhancement. New *combed* features that were first seen on 22:01 January 12th 2007 have had their theoretical positions tracked backwards within the data and are shown in red. These features would have been sunward aligned 8 to 14 hours previously. Note that features on the far left of the temporal maps are artefacts from the overexposed region near the comet's nucleus.

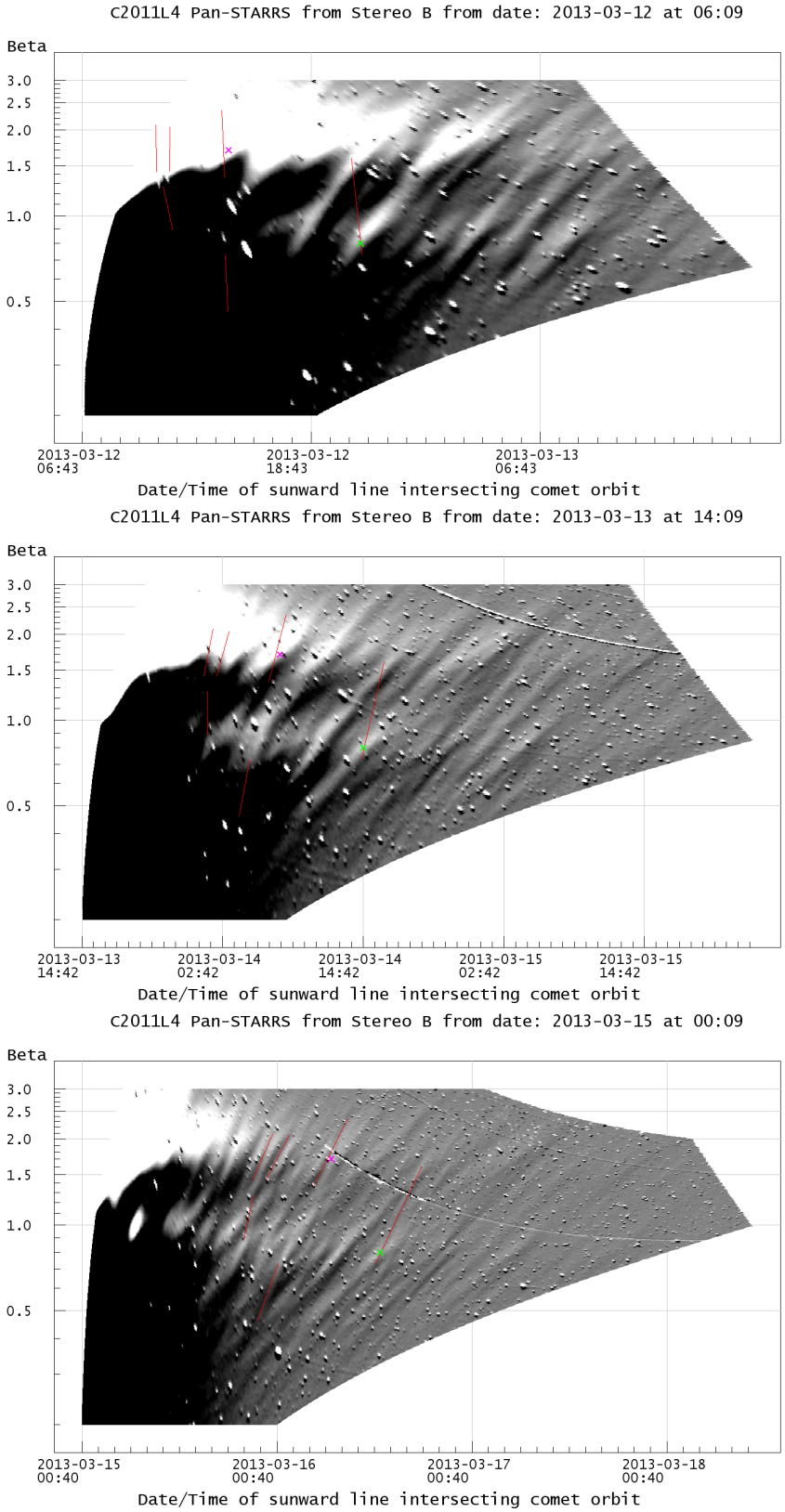

Figure 18: Three sunward-aligned temporal maps of C/2011 L4's main dust tail region as seen by HI-1B with coarse-scale difference enhancement. New *combed* features that were first seen throughout January 14th 2007 have had their theoretical positions tracked backwards within the data and are shown in red. These features would have been sunward aligned 1 to 3 days previously.

A reasonable assumption is probably that any reorganisation of the dust that can be visually resolved is the main component of the full reorganisation process. There is no reason to suspect that once the Lorentz force acting on the dust has changed direction, its effects would not be immediately felt. Horanyi and Mendis (1987) predicted that orientation changes in dust tails composed of 0.1 μm grains would be visible within a few days. Considering this, whilst it seems possible that combed features at McNaught could have had a purely radial origin with respect to the sun, the long gaps of 2 to 3 days between a possible radial orientation and the visible onset of feature evolution at C/2011 L4 would appear to rule out such a phenomenon as an explanation for the alignment of combed features. Additionally, there is no good physical explanation that can be proposed for such sunward aligned behaviour; optical thickness effects acting on clouds of dust, e.g. by lowering the effective β_r of shadowed dust regions (Notni and Thaenert, 1988), are probably not a factor here as the dust is too dispersed, and the evolved regions of the dust tail concerned are clearly optically-thin.

6.2. Does the alignment match a solar wind cause?

Given that the reorganisation process appears to correlate strongly with crossings of the HCS, it seems reasonable to assume that the structure of the combed features is therefore also associated with the solar wind conditions. Furthermore, assuming that any features are created by a discrete structure moving with the solar wind, the exact orientation of features would depend on the path of this structure through the comet's tail. A dust tail feature's orientation would be therefore dependent on the speeds of the solar wind as well as those of the comet and its dust tail. This is illustrated in Figure 19.

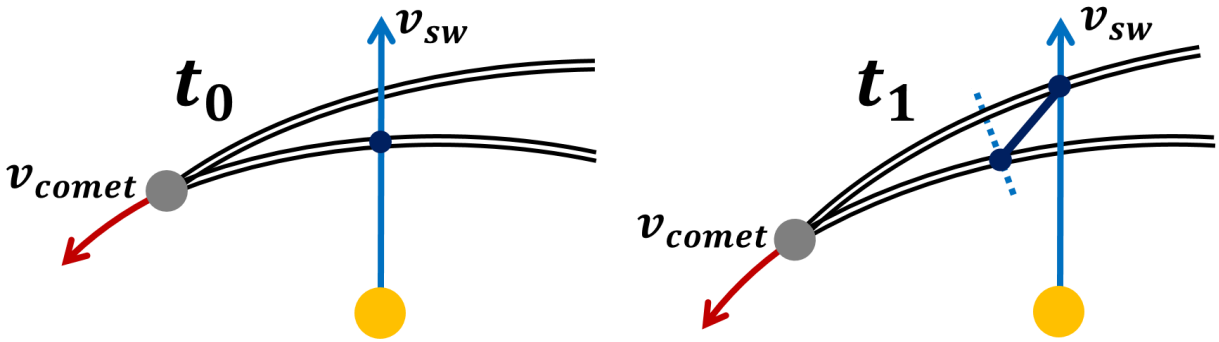

Figure 19: Diagram showing how combed features with a solar wind cause would have orientations depending on the solar wind speed. The angle at which combed features form would be a function of the solar wind speed and the speed of the comet and its tail. Slower solar wind speeds would mean longer between t_0 when the solar wind enters the tail and t_1 when it exits the tail. Slower solar winds would therefore be associated with shallower-inclined features and vice versa.

As the speeds of dust across the whole tail are a known quantity from the Finson-Probstein model, it is therefore possible to calculate the path of solar wind features across the tail for a range of solar wind speeds. This allows for a mapping of the tail to be displayed in the modified (β_r, θ_{corr}) phase space, where each θ_{corr} corresponds to a near radial path taken by a solar wind feature. In other words, each θ_{corr} corresponds to the original heliolongitude of a stream of solar wind within the comet's frame of reference.

This is not as simple as extracting the solar wind speeds directly from the orientation of the features, because again this interpretation is dependent on the time at which the feature is deemed to have been created, and without knowing the timescale for feature formation this remains hard to pinpoint. Instead these maps provide a lower bound on the solar wind speed associated with a combed feature. The slower the solar wind, the larger angle the feature would have to the radial sunward direction. However, larger angles are also created as features evolves, due to their Finson Probstein motion. Therefore the minimum angle each feature makes with the sunward direction – seen when features first appear – gives a minimum limit on the solar wind speed. Larger solar wind speeds cannot be ruled out for the same reasons detailed in section 6.1; they could have been correct at the time of the feature formation, after which the motion of the dust changes the angle at which features appear. The larger the solar wind speed, the longer

the possible timescale between feature formation and manifestation. The upper limit on these timescales is given by the case where $v_{sw} \to \infty$, which corresponds to fully sunward aligned feature formation as investigated previously.

Visually, this process involves varying the solar wind speed of the correction applied to a temporal map. The solar wind speed for which observed features align vertically gives the minimum possible causal solar wind speed; applying a smaller solar wind speed results in an over-correction. Figures 20 and 21 show several solar wind corrected temporal maps for two frames taken from the two datasets at C/2006 P1 and C/2011 L4 respectively. These correspond to the frames from figures 15 and 16 where combed features first clearly appeared.

An animation showing these corrected temporal maps for a range of solar wind speeds for C/2006 P1 as seen in Figure 20 is available here:

`https://doi.org/10.5522/04/17082155`

An animation showing these corrected temporal maps for a range of solar wind speeds C/2011 L4 as seen in Figure 21 is available here:

`https://doi.org/10.5522/04/17082161`

Figures 20 and 21 show that for feature alignment explainable by a solar wind cause, the minimum speed of the solar wind must have been around 500 km s^{-1} for C/2006 P1 and 190 km s^{-1} for C/2011 L4. These two different speeds correspond to the orientation of combed features at C/2006 P1 being slightly closer to the radial direction.

These results allow for an interesting comparison to the CORHEL simulated solar wind data for both comets. At C/2011 L4, the CORHEL data model shown in Figure 14 suggest that the radial solar wind speeds remained fairly constant for the comet during the HCS crossings at around 280 km s^{-1}; including within the tail at dust points **P** and **G**, providing any perturbations to the solar wind from the comet's own plasma environment were minimal. This is certainly consistent with the results obtained here, and would correspond to a short non-visible timescale during the formation of the combed features.

The C/2006 P1 encounter is less consistent. As seen in Figure 18 of Price et al. (2019), the CORHEL simulated radial solar wind speed at the HCS crossing was estimated to be 300 km s^{-1} for the nucleus, as it passed through the streamer belt. This would appear to disagree with the orientations of the combed features seen here which suggest the features formed at radial solar wind speed of at least 500 km s^{-1}. However, the radial solar wind speed quickly rose to above 500 km s^{-1} 12 hours after the HCS crossing. If the combing structure is imprinted not immediately, but shortly after the HCS crossing, then the speeds calculated here may have been possible during the reorganisation process. Another factor is the width of the dust tail in the radial direction; which was at least 0.1 AU in the main part of the tail. A solar wind feature travelling at 500 km s^{-1} would have taken 8 hours to cross the full tail. The assumption of a fixed solar wind speed across all parts of the tail, whilst a reasonable first order approximation, is certainly an over-simplification. Our model here has also assumed a purely radial solar wind, whereas in reality the solar wind also has small non radial components. A small non radial component acting over a significant distance of 0.1 AU could well have a noticeable effect on the path of a solar wind feature through the tail and hence combed feature orientation.

Overall, our results do not appear to confirm definitively that the alignments of combed features have a solar wind cause, but neither is it possible to rule out such a cause. The C/2011 L4 observations in particular appear to be consistent with such a cause.

7. Conclusions

7.1. Dust and solar wind interaction at C/2011 L4

The results presented here for C/2011 L4 provide further confirmation that solar wind conditions have a noticeable effect on dust tail structure. This second observed correlation of striae reorganisation behaviour with crossing of the HCS – as predicted by Horanyi and Mendis (1987) – appears to reinforce the conclusions drawn in Price et al. (2019). Again, these observations appear to show that grains that may be susceptible to electrodynamic effects are larger than previously anticipated.

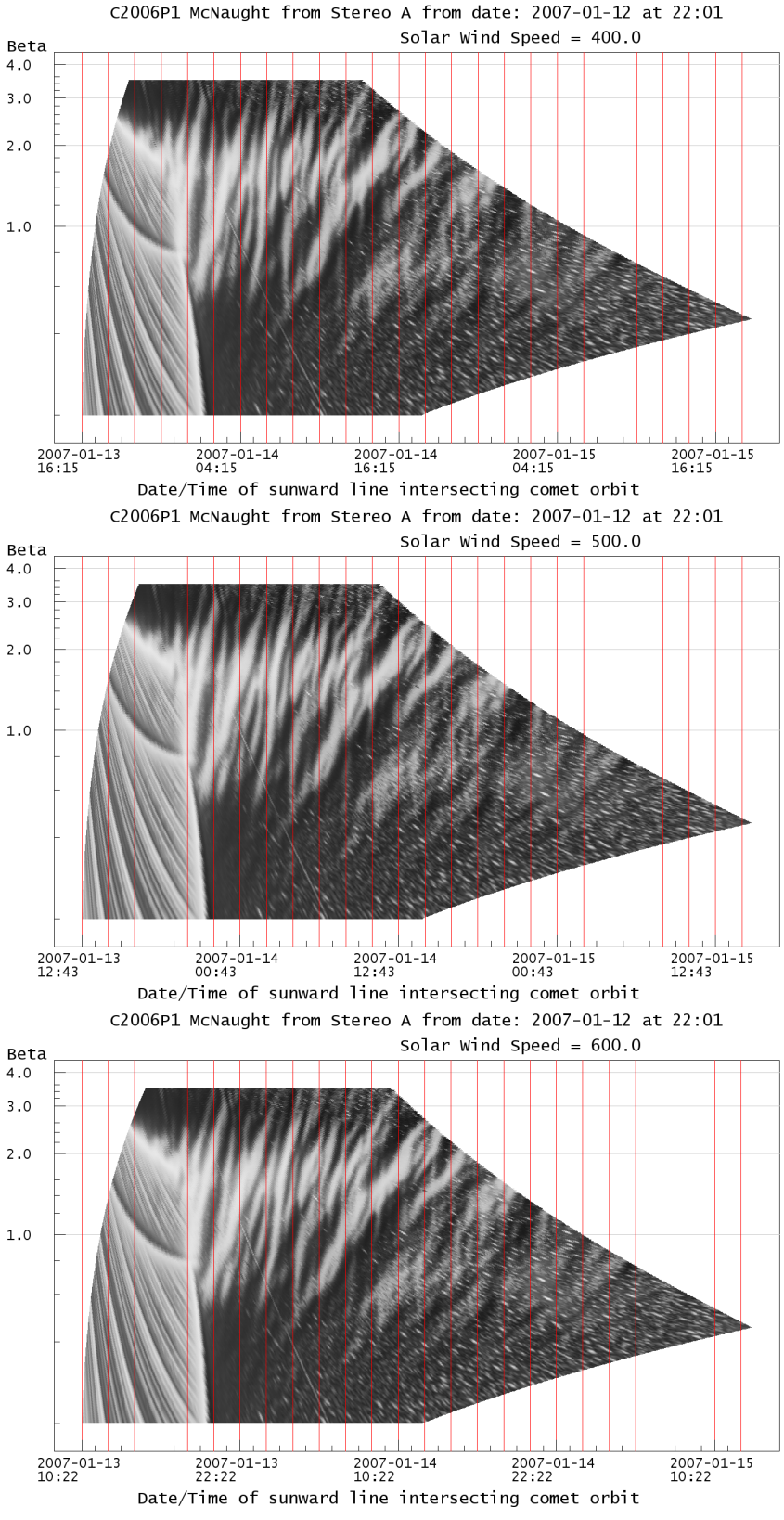

Figure 20: Three solar wind aligned temporal maps of C/2006 P1's main dust tail region as seen by HI-1A with MGN enhancement. The x-axis corresponds to the paths through the comet tail taken by solar wind features of the annotated speed. Solar wind speeds of 500 km s^{-1} and above are compatible with the orientation of the combed features that form in C/2006 P1's dust tail. Note that features on the far left of the temporal maps are artefacts from the overexposed region near the comet's nucleus.

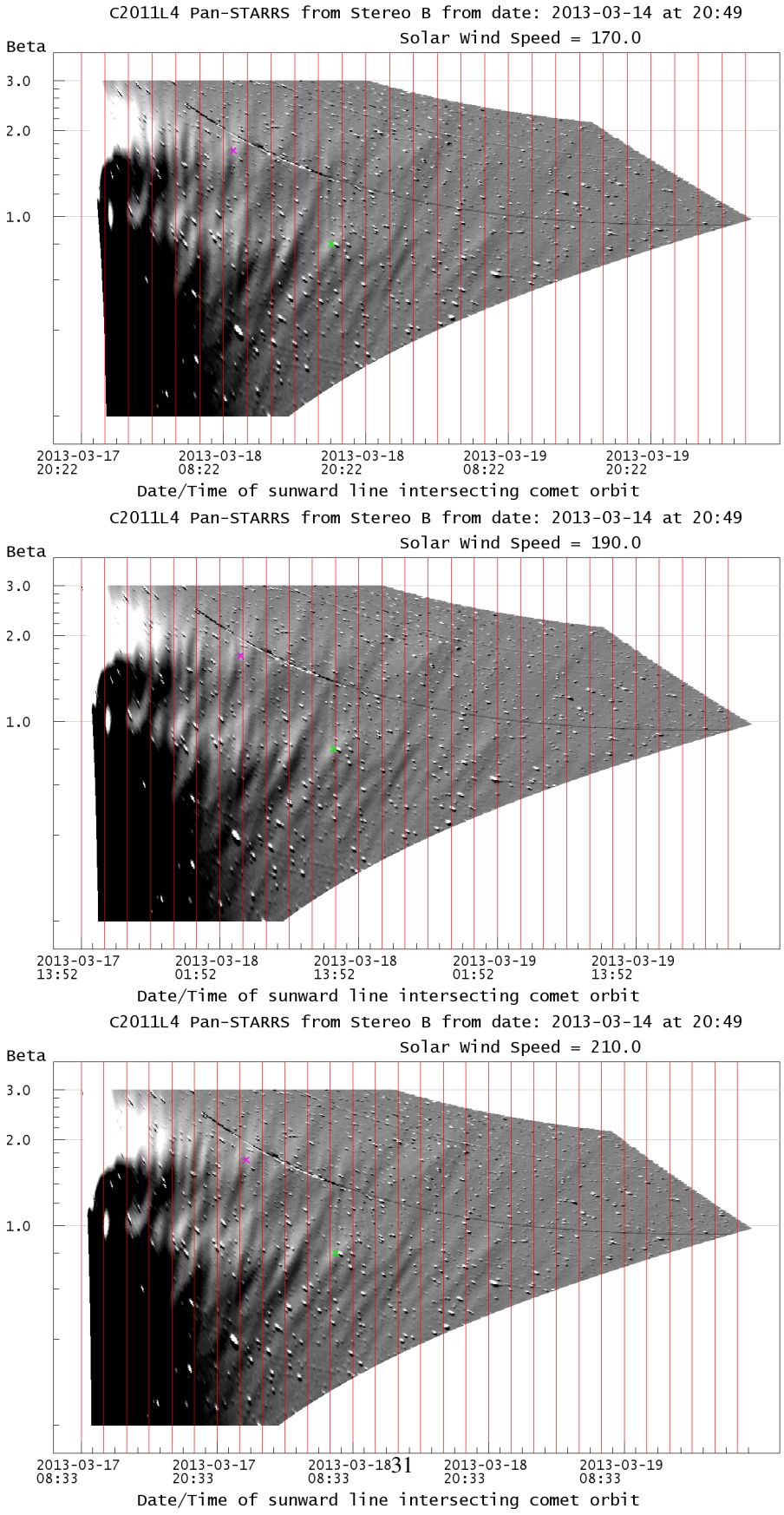

Figure 21: Three solar wind aligned temporal maps of C/2011 L4's main dust tail region as seen by HI-1B with coarse-scale difference enhancement. The x-axis corresponds to the paths through the comet tail taken by solar wind features of the annotated speed. Solar wind speeds of 190 km s^{-1} and above are compatible with the orientation of the combed features that form in C/2011 L4's dust tail.

7.2. Similarities and differences between reorganisation events at C/2006 P1 and C/2011 L4

The broad similarities between the striae formation and reorganization at both comets – in terms of visible behaviour and its correlation with solar wind conditions – mean we have assumed the underlying physics between the two events is broadly similar. We now briefly compare and contrast the two events. Table 2 summarises the main parameters for the nucleus of each comet during the HCS crossing events. The observations made here have benefited from the similar comet-spacecraft distances for both comets, as well as orbit plane angle values conducive to the success of the temporal mapping method. The higher production rate at C/2006 P1 meant that its dust tail was larger, longer lasting, and imaged much more clearly than that of C/2011 L4. Despite this, both comets had remarkably similar tails in terms of their morphologies. Both displayed a bimodal β_r distribution and were extensively striated with no clear pattern in the temporal distribution of striae, with the exception of some ground based images of C/2011 L4. For both comets, a HCS crossing occurred shortly after perihelion, and generally each comet behaved similarly during the crossing events, with combing behaviour producing new off-radial striae features that spanned across the existing bimodal striated tail.

		C/2011 L4 Pan-STARRS	
Nucleus Parameters	**C/2006 P1 McNaught**	**1**	**2**
Time	2007-01-13 03:00	2013-03-12 05:00	2013-03-13 17:30
Heliospheric Distance (AU)	0.171	0.308	0.321
Days after perihelion	0.326	2.038	3.559
Max water production rate (~molecules~s^{-1})	5.48×10^{31}	1×10^{30}	
B_ϕ (nT)	~10	~5	
v_r (kms^{-1})	300	280	
Solar cycle phase	Minimum	Maximum	
Observing Spacecraft	STEREO-A	STEREO-B	
Distance to spacecraft (AU)	0.845	0.809	0.793
Orbit plane angle	29.6	-46.6	-45.6

Table 2: List of key parameters at the nucleus during the three HCS crossing and striae reorganisation events. Values informed by CORHEL simulations – including the times of the HCS crossings – are only rough estimates. The exact parameters for dust in the tail will be of course different, e.g. see Figure 14. Max water production rates are from Combi et al. (2011) and Combi et al. (2014), respectively.

However, these two encounters took place at different stages of the solar cycle. C/2006 P1 encountered a solar wind typical of solar minimum; a HCS at low latitudes embedded in a streamer belt of slow solar wind, with faster winds outside of this region. Six years later, C/2011 L4 encountered a heliosphere near solar maximum. Slower wind speeds were seen throughout, and with less of a dipolar structure, the HCS was more complex in shape, and covered a wider range of latitudes, with the comet making two HCS crossings. The lower activity and larger heliospheric distance of C/2011 L4 relative to C/2006 P1 also meant that structural changes were slightly harder to observe.

7.3. Combed features at C/2011 L4 and C/2006 P1

At both comets, the reorganisation process clearly created distinct new structures within the dust tail. The creation of initially *interleaved* structures eventual leads to the formation of new, sunward pointing *combed* features. However, the process was much less pervasive throughout the tail at C/2011 L4, compared to C/2006 P1. Rather than a large number of disrupted sunward pointing features mixed with original striae, C/2011 L4 showed only a few prominent sunward pointing features, which were unevenly spaced. Some pre-existing striae appeared to stay much more well preserved, apparently unaffected by the redistribution occurring elsewhere in the tail. This is probably best explained again by the double HCS crossing, the comparatively lower activity of the comet, and the ~~higher~~ heliocentric distance.

The orientations of the new *combed* striae were examined both for C/2006 P1 and C/2011 L4. These new features were aligned slightly off the radial direction from the sun. The positions of these features were traced backwards

in time before they became visible and for both comets would have been completely radially aligned at some point. For C/2006 P1 this would correspond to a formation time of 8 to 14 hours. Features at C/2011 L4 formed a larger angle to the sunward direction and so would only have been radially aligned after a longer delay of 1 to 3 days. This excessively large timescale would appear to rule out a radial formation process for C/2011 L4.

An alternative hypothesis is that combed features might have formed at angles corresponding to the paths taken by solar wind features through the dust tail, with features' orientations therefore giving a lower bound for the solar wind speed at which this would have taken place. The lower bound at C/2011 L4 of 190 km s^{-1} is compatible with the simulated solar wind speeds during its HCS encounter. However, the minimum solar wind speed for such behaviour at C/2006 P1 of 500 km s^{-1} seems too large compared with the speeds found within the streamer belt where this comet would have crossed the HCS. However, it is comparable to the speeds seen in the rest of the solar wind, which the comet was simulated to have entered some 12 hours after the HCS crossing. Additionally, it is worth considering that the CORHEL model is only a simulation. It does not necessarily represent real-world, definitive solar wind measurements, although there is no reason either to strongly doubt its accuracy.

Overall, it is not possible to confirm that the alignment of the newly formed combed features matches well to a solar wind cause. However, in the absence of any other plausible explanation, and considering the strong correlation of the onset of the combing process with the crossing of the HCS, it seems likely that the solar wind conditions are in some way associated with the forming of new combed striae features. We discuss this and other possible combing mechanisms below.

8. Outstanding Questions

Following on from the above conclusions, two outstanding questions remain are now briefly considered:

- What is the physical mechanism behind the formation of new combed features after a HCS crossing reorganisation event?
- What connection, if any, does this mechanism have with the original formation process for striae?

8.1. Formation of new combed features

Understanding how distinct combed features are formed at C/2006 P1 and C/2011 L4 will be key to understanding the general mechanics of the HCS crossing and reorganisation events. Following on from the work presented in Price et al. (2019) and here, there are several things that are known about these features:

- The appearance of combed features occurs in already striated tails and appears to be correlated with crossing of the HCS.
- Combed features are not formed in any strict order relating to dust feature age. Although this also appears to be the case for striae as well (Price et al., 2019), exceptions to chronological striae formation only happen for dust several hours younger at most; most feature formation is still roughly chronological. Formation of combed features can occur in any order, for example to dust many days older than other younger dust within the tail.
- Combed features can form over the whole tail or just one or several parts.
- Combed features often appear to cross over several pre-existing striae. Conversely, each pre-existing stria may be intersected by multiple combed features.
- Combed features can appear as bright features themselves, or as gaps in the fine structure of the tail.
- Approximate dimensions of these features or gaps can also be obtained from the STEREO data. They have lengths in the range of 0.03 to 0.05 AU (4.5 to 7.5 $\times 10^6$ km), and widths in the range of (1 to 2) $\times 10^5$ km.
- Combed features have been observed at heliocentric distances of 0.17 to 0.32 AU; around and within the orbit of Mercury.

- Combed features have orientations that point slightly off the sunward radial direction when formed. Such an orientation could indicate a radial formation some time before features become visible, or a formation caused by a feature moving through the tail at a speed similar to that of the solar wind. There is mixed evidence for both possibilities.

- Timescales for the formation of combed features are **not** well known. The formation timescales of striae themselves can however be provided based on the observed formation times reported by Price et al. (2019).

Correspondingly, there could be a number of different formation mechanisms for these combed features. A few suggested ones are:

- They form in the same manner as striae are thought to form; through fragmentation triggered in some way by the HCS crossing.

- They form as a consequence of existing striae sub-structure. If original striae form through a multiple stage fragmentation i.e. as per Nishioka (2021) or Steckloff and Jacobson (2016), each stria may contain sub structure; when following the last occurrence of fragmentation, daughter dust of varying β_r spreads out over one part of the stria to form a "sub-stria" structure. Crossing the HCS causes each of these "sub-stria" to undergo an orientation change – as detailed in Horanyi and Mendis (1987) – and these re-orientated "sub-stria" form combed features.

- They form due to structures within the solar wind itself. Following the HCS crossing, as dust undergoes an orientation change as per Horanyi and Mendis (1987), it could be particularly susceptible to variations in the HMF. Structure within the solar wind may be imprinted onto the dust as varying strengths of the magnetic field affect some regions of the tail more strongly than others.

A fragmentation based mechanism seems particularly unlikely for several reasons. The strongest evidence against this seems to be the large distances at which features first appear, particularly for C/2006 P1. Striae formation mechanisms rely on the quick increase of scale of the dust tail as features of different β_r spread out over time. This allows small clouds of dust to fragment and eventually become large scale structures within the tail. When combed features manifest, they appear from parts of the dust tail that already span large distances. Striae also generally tend to form roughly chronologically, and when they do not it is only from dust several hours younger at most. Conversely, combed features appear to be much more spatially-bound as opposed to temporally-bound in their formation.

A striae sub-structure approach seems more promising, but again has some issues. Even if there is existing sub-structure within one stria that can contribute to a combed feature, such features appear to sometimes comprise material from many different striae. It is difficult to see how such an explanation can involve material from different original striae linking together to form a new combed feature. It is also hard to explain how some combed features manifest as dark gaps rather than bright features themselves.

This leaves a solar wind structure explanation. This seems a promising choice, as the reorganisation process is already known to be linked to one aspect of the solar wind structure; the position of the HCS. Such an explanation would require some kind of sub-structure within the solar wind, thus allowing local variations in solar wind conditions to form the new combed structure.

Flux tubes seem a promising candidate for such features. These are long, thin, roughly cylindrical regions of space with all their sides orientated parallel to magnetic field lines. As a consequence of Gauss's law of magnetism, flux through any section of the tube is conserved. They present a physically meaningful way to partition a magnetic field under study; and are isolated entities themselves governed by a Newtonian equation of motion (Schrijver and Siscoe, 2009). The solar wind is often referred to as a sea of entangled flux tubes, sometimes described as a "spaghetti". At 1 AU, flux tubes are thought to have a median width of 4.4×10^5 km, similar to the width of the combed features (Borovsky, 2008). However, if flux tubes are present in all parts of the solar wind, then there is a question of why their influence is not seen on other dust within this part of the solar system e.g. in zodiacal dust. The lack of evidence of such structuring in the zodiacal cloud may be that this is viewed as an optically-thin structure, with the optical path of the viewer passing through a great distance, over which any localized structuring is of very low contrast due to light scattered from dust further and closer to the observer than the feature itself.

Another candidate structure might be flux ropes, which are formed from twisted flux tubes in certain specific circumstances. There is also structure in the young solar wind when it has just left the corona. This includes bright radial

features known as *striae* (not to be confused with cometary striae). Other features include local density enhancements such as *Sheeley Blobs* and *Viall Puffs* (DeForest et al. 2016; DeForest et al. 2018, and references therein). However, these structures evolve rapidly with heliocentric distance, particularly as the flow of the solar wind becomes more turbulent further from the sun (DeForest et al., 2016). A requirement for any potential explanation of combing is that it must be explainable over a range of heliocentric distances around and within the orbit of Mercury.

If it is the case that solar wind structure is the cause of combing, then there is a question of how this relates to striae formation. An Occam's Razor approach to explain both features from the same mechanism is appealing, but of course this may be a fallacy. It could be asked if solar wind structure has any role in the formation of normal striae. The alignment of the structures when both features first appear is similar, pointing in the same orientation slightly off radially. However, there appears to be more variation in the alignment when striae form; some are completely radial, whereas others curve relative to the radial direction. This behaviour is not seen in combed features. The formation of the "notch" – a prominent gap in the fine structure of the tail of C/2006 P1 for dust ejected from the nucleus around the time of the HCS crossing – seems to indicate that whatever process which causes combing can have some effect on striae formation.

There is not enough evidence to make any definitive statement on the origin of combed features here. In the authors' opinion, the best hypothesis is probably one involving solar wind structure. Further work required to address this is suggested below.

8.2. Future work

The temporal mapping technique described in Price et al. (2019) has the potential to be applied to any dataset of cometary dust tail images. At the time of writing, the comets studied in Price et al. (2019) and this work, together with C/2002 V1 NEAT to appear in a forthcoming publication, are the only comets for which SOHO and STEREO datasets provide dust tail images with enough detail to resolve fine structure. Nevertheless, the technique remains available for use on existing and future ground or space based images.

Improvements to the temporal mapping technique could be made by using a more precise photometric treatment of temporally mapped data. This would involve normalising the brightness of every part of the temporal map relative to the scale of the original mapped area and the bandpass of the instrument. A more formal treatment of the data would also allow for normalisation based on known dust phase functions. These modifications should allow for better correlation between temporal maps where observer geometry is vastly different, as was the case for space and ground based data of C/2011 L4.

Resolution of the physics behind dust tail reorganisation and other dust and magnetic field structure interactions will require a thorough and interdisciplinary approach, rather than the cometary physics aligned path taken here. Solving this mystery will require understanding of several areas of physics far beyond the scope of this work and in some cases beyond existing literature. These will include:

- A more conclusive model of striae formation mechanics and dust fragmentation behaviour. Currently there is no consensus on the exact mechanism through which striae form, and therefore the properties and distribution of dust within the striated dust tail is not particularly well constrained. Price et al. (2019) and this work provide some clues on which already suggested mechanisms may be most valid. In observing striae formation for this first time and considering the sunward radial alignment of features it appears that the shadowing hypothesis of Froehlich and Notni (1988) may be important. Additionally the interleaved nature of the HCS crossing reorganisation process suggests that models which allow for more mixed dust properties along a stria are more accurate such as those by Nishioka and Watanabe (1990), Nishioka (1998), and Nishioka (2021). Valuable data from the Rosetta mission have yet to make their way into the literature on this topic of macroscopic features in extensive dust tails. They should hopefully allow for the refinement of striae formation models, particularly in consideration of the wealth of data on dust properties, which will hopefully constrain models of dust fragmentation. However, there are some limitations on what can be learned from a short period comet such as 67P. Resolving some questions about the dynamically new long period comets considered here – for example the number and density of ejected boulders compared with a Steckloff and Jacobson (2016) type formation mechanism – might require a bespoke mission to such a comet. This should be provided by the ESA/JAXA *Comet Interceptor* mission, launching in 2029 (Snodgrass and Jones, 2019).

- A detailed appreciation of the magnetic structure of the heliosphere at low heliocentric distances i.e. around and within the orbit of Mercury. Whilst there is existing theory on the plasma environment of this part of the solar system, it should only improve as results continue to come in from the Parker Solar Probe (Fox et al., 2016) and Solar Orbiter (Müller et al., 2020) missions. Additionally, the 7 year proposed mission durations for both spacecraft should allow them to study any effects caused by the solar cycle, the understanding of which may be necessary for resolving the dust tail physics at both C/2006 P1 and C/2011 L4.

- A good understanding of the interaction of solar wind plasma with dust in the tail. This will require appreciation of the field of dusty plasmas within a space physics context.

Solving the mysteries of how comet dust tails interact with the solar wind will be difficult. It is not a great omen that after more than 40 years there is no definitive answer on how striae themselves are formed. Still, when single point measurements are all that is available for this region of the inner heliosphere, this work suggest a tantalising prospect; that comet dust tails may provide an opportunity to characterise larger scale solar wind structure within this region.

9. Acknowledgements

OP is supported by a UK Science and Technology Facilities Council (STFC) PhD studentship. GHJ is grateful to STFC for partial support through consolidated grants ST/K000977/1 and ST/S000240/1. KB is supported by the NASA-Funded Sungrazer Project. The SOHO/LASCO data used here are produced by a consortium of the Naval Research Laboratory (USA), Max-Planck-Institut für Sonnensystemforschung (Germany), Laboratoire d'Astronomie (France), and the University of Birmingham (UK). SOHO is a project of international cooperation between ESA and NASA. The STEREO/SECCHI data are produced by an international consortium of the NRL (USA), LMSAL (USA), NASA-GSFC (USA), RAL (UK), University of Birmingham (UK), MPS (Germany), CSL (Belgium), IOTA (France), and IAS (France). *Astrometry.net* is funded by the US National Science Foundation, the US National Aeronautics and Space Administration, and the Canadian National Science and Engineering Research Council. SOLIS magnetograms are produced cooperatively by NSF/NSO and NASA/LWS. The National Solar Observatory (NSO) is operated by the Association of Universities for Research in Astronomy, Inc., under cooperative agreement with the National Science Foundation. Simulation results have been provided by the Community Coordinated Modeling Center at Goddard Space Flight Center through their public Runs on Request system (*ccmc.gsfc.nasa.gov*). The CORHEL/MAS/WSA/ENLIL Model was developed by J. Linker, Z. Mikic, R. Lionello, P. Riley, N. Arge, D. Odstrcil at PSI, AFRL & U.Colorado. This research made use of Astropy, a community-developed core Python package for Astronomy (Astropy Collaboration et al., 2013, 2018). This research used version 3.1.3 (Mumford et al., 2022) of the SunPy open source software package (The SunPy Community et al., 2020).

References

Astropy Collaboration, Price-Whelan, A.M., Sipőcz, B.M., Günther, H.M., Lim, P.L., Crawford, S.M., Conseil, S., Shupe, D.L., Craig, M.W., Dencheva, N., Ginsburg, A., VanderPlas, J.T., Bradley, L.D., Pérez-Suárez, D., de Val-Borro, M., Aldcroft, T.L., Cruz, K.L., Robitaille, T.P., Tollerud, E.J., Ardelean, C., Babej, T., Bach, Y.P., Bachetti, M., Bakanov, A.V., Bamford, S.P., Barentsen, G., Barmby, P., Baumbach, A., Berry, K.L., Biscani, F., Boquien, M., Bostroem, K.A., Bouma, L.G., Brammer, G.B., Bray, E.M., Breytenbach, H., Buddelmeijer, H., Burke, D.J., Calderone, G., Cano Rodríguez, J.L., Cara, M., Cardoso, J.V.M., Cheedella, S., Copin, Y., Corrales, L., Crichton, D., D'Avella, D., Deil, C., Depagne, É., Dietrich, J.P., Donath, A., Droettboom, M., Earl, N., Erben, T., Fabbro, S., Ferreira, L.A., Finethy, T., Fox, R.T., Garrison, L.H., Gibbons, S.L.J., Goldstein, D.A., Gommers, R., Greco, J.P., Greenfield, P., Groener, A.M., Grollier, F., Hagen, A., Hirst, P., Homeier, D., Horton, A.J., Hosseinzadeh, G., Hu, L., Hunkeler, J.S., Ivezić, Ž., Jain, A., Jenness, T., Kanarek, G., Kendrew, S., Kern, N.S., Kerzendorf, W.E., Khvalko, A., King, J., Kirkby, D., Kulkarni, A.M., Kumar, A., Lee, A., Lenz, D., Littlefair, S.P., Ma, Z., Macleod, D.M., Mastropietro, M., McCully, C., Montagnac, S., Morris, B.M., Mueller, M., Mumford, S.J., Muna, D., Murphy, N.A., Nelson, S., Nguyen, G.H., Ninan, J.P., Nöthe, M., Ogaz, S., Oh, S., Parejko, J.K., Parley, N., Pascual, S., Patil, R., Patil, A.A., Plunkett, A.L., Prochaska, J.X., Rastogi, T., Reddy Janga, V., Sabater, J., Sakurikar, P., Seifert, M., Sherbert, L.E., Sherwood-Taylor, H., Shih, A.Y., Sick, J., Silbiger, M.T., Singanamalla, S., Singer, L.P., Sladen, P.H., Sooley, K.A., Sornarajah, S., Streicher, O., Teuben, P., Thomas, S.W., Tremblay, G.R., Turner, J.E.H., Terrón, V., van Kerkwijk, M.H., de la Vega, A., Watkins, L.L., Weaver, B.A., Whitmore, J.B., Woillez, J., Zabalza, V., Astropy Contributors, 2018. The Astropy Project: Building an Open-science Project and Status of the v2.0 Core Package. Astron. J. 156, 123. doi:10.3847/1538-3881/aabc4f, arXiv:1801.02634.

Astropy Collaboration, Robitaille, T.P., Tollerud, E.J., Greenfield, P., Droettboom, M., Bray, E., Aldcroft, T., Davis, M., Ginsburg, A., Price-Whelan, A.M., Kerzendorf, W.E., Conley, A., Crighton, N., Barbary, K., Muna, D., Ferguson, H., Grollier, F., Parikh, M.M., Nair, P.H., Unther, H.M., Deil, C., Woillez, J., Conseil, S., Kramer, R., Turner, J.E.H., Singer, L., Fox, R., Weaver, B.A., Zabalza, V., Edwards, Z.I., Azalee Bostroem, K., Burke, D.J., Casey, A.R., Crawford, S.M., Dencheva, N., Ely, J., Jenness, T., Labrie, K., Lim, P.L., Pierfederici, F., Pontzen, A., Ptak, A., Refsdal, B., Servillat, M., Streicher, O., 2013. Astropy: A community Python package for astronomy. Astron. & Astroph. 558, A33. doi:10.1051/0004-6361/201322068, arXiv:1307.6212.

Bewsher, D., Brown, D.S., Eyles, C.J., Kellett, B.J., White, G.J., Swinyard, B., 2010. Determination of the photometric calibration and large-scale flatfield of the STEREO heliospheric imagers: I. HI-1. Solar Physics 264, 433–460. doi:10.1007/s11207-010-9582-8.

Borovsky, J.E., 2008. Flux tube texture of the solar wind: Strands of the magnetic carpet at 1 AU? Journal of Geophysical Research: Space Physics 113, A08110. doi:10.1029/2007JA012684.

Combi, M.R., Bertaux, J.L., Quémerais, E., Ferron, S., Mäkinen, J.T.T., Aptekar, G., 2014. Water Production in Comets C/2011 L4 (PanSTARRS) and C/2012 F6 (Lemmon) from observations with SOHO/SWAN. The Astronomical Journal 147, 126. URL: http://stacks.iop.org/1538-3881/147/i=6/a=126?key=crossref.0c9cca15d6ec4b9379b0d44eea224ffb, doi:10.1088/0004-6256/147/6/126.

Combi, M.R., Boyd, Z., Lee, Y., Patel, T.S., Bertaux, J.L., Quémerais, E., Mäkinen, J.T.T., 2011. SOHO/SWAN observations of comets with small perihelia: C/2002 V1 (NEAT), C/2002 X5 (Kudo-Fujikawa), 2006 P1 (McNaught) and 96P/Machholz 1. Icarus 216, 449–461. doi:10.1016/j.icarus.2011.09.019.

Cometary Science Archive, 2021. Cometary Science Archive: Comet C/2011 L4 (PANSTARRS). http://csc.eps.harvard.edu/2011L4/index.html. Accessed: 2021-04-11.

Cremonese, G., Boehnhardt, H., Crovisier, J., Rauer, H., Fitzsimmons, A., Fulle, M., Licandro, J., Pollacco, D., Tozzi, G.P., West, R.M., 1997. Neutral Sodium from Comet Hale-Bopp: A Third Type of Tail. The Astrophysical Journal Letters 490, L199.

DeForest, C.E., Howard, R.A., Velli, M., Viall, N., Vourlidas, A., 2018. The Highly Structured Outer Solar Corona. The Astrophysical Journal 862, 18. doi:10.3847/1538-4357/aac8e3.

DeForest, C.E., Matthaeus, W.H., Viall, N.M., Cranmer, S.R., 2016. Fading Coronal Structure and the Onset of Turbulence in the Young Solar Wind. The Astrophysical Journal 828, 1–16. doi:10.3847/0004-637X/828/2/66, arXiv:1606.07718.

Eyles, C., Harrison, R., Davis, C., Waltham, N., Shaughnessy, B., Mapson-Menard, H., Bewsher, D., Crothers, S., Davies, J., Simnett, G., et al., 2009. The heliospheric imagers onboard the stereo mission. Solar Physics 254, 387–445.

Ferrín, I., 2014. The location of Oort cloud comets C/2011 L4 panstarrs and C/2012 S1 ISON on a comet evolutionary diagram. Monthly Notices of the Royal Astronomical Society 442, 1731–1754. doi:10.1093/mnras/stu820.

Finson, M., Probstein, R., 1968. A theory of dust comets. I. Model and equations. The Astrophysical Journal 154, 327–352.

Fox, N.J., Velli, M.C., Bale, S.D., Decker, R., Driesman, A., Howard, R.A., Kasper, J.C., Kinnison, J., Kusterer, M., Lario, D., Lockwood, M.K., McComas, D.J., Raouafi, N.E., Szabo, A., 2016. The Solar Probe Plus Mission: Humanity's First Visit to Our Star. Space Science Reviews 204, 7–48. URL: http://dx.doi.org/10.1007/s11214-015-0211-6, doi:10.1007/s11214-015-0211-6.

Froehlich, H.E., Notni, P., 1988. Radiation pressure — a stabilizing agent of dust clouds in comets? Astronomische Nachrichten: A Journal on all Fields of Astronomy 309, 147–155. doi:10.1002/asna.2113090211.

Fulle, M., 2004. Motion of cometary dust, in: Comets II. Citeseer, pp. 565–575.

Fulle, M., Leblanc, F., Harrison, R.A., Davis, C.J., Eyles, C.J., Halain, J.P., Howard, R.A., Bockelée-Morvan, D., Cremonese, G., Scarmato, T., 2007. Discovery of the Atomic Iron Tail of Comet MCNaught Using the Heliospheric Imager on STEREO. The Astrophysical Journal Letters 661, L93–L96. doi:10.1086/518719.

Gustafson, B.A.S., 1994. Physics of Zodiacal Dust. Annual Review of Earth and Planetary Sciences 22, 553–595. doi:10.1146/annurev.ea.22.050194.003005.

Horanyi, M., Mendis, D.A., 1987. The effect of a sector boundary crossing on the cometary dust tail. Earth, Moon, and Planets 37, 71–77. doi:10.1007/BF00054325.

Howard, R.A., Moses, J.D., Vourlidas, A., Newmark, J.S., Socker, D.G., Plunkett, S.P., Korendyke, C.M., Cook, J.W., Hurley, A., Davila, J.M., Thompson, W.T., St Cyr, O.C., Mentzell, E., Mehalick, K., Lemen, J.R., Wuelser, J.P., Duncan, D.W., Tarbell, T.D., Wolfson, C.J., Moore, A., Harrison, R.A., Waltham, N.R., Lang, J., Davis, C.J., Eyles, C.J., Mapson-Menard, H., Simnett, G.M., Halain, J.P., Defise, J.M., Mazy, E., Rochus, P., Mercier, R., Ravet, M.F., Delmotte, F., Auchere, F., Delaboudiniere, J.P., Bothmer, V., Deutsch, W., Wang, D., Rich, N., Cooper, S., Stephens, V., Maahs, G., Baugh, R., McMullin, D., Carter, T., 2008. Sun Earth Connection Coronal and Heliospheric Investigation (SECCHI). Space Science Reviews 136, 67–115. doi:10.1007/s11214-008-9341-4.

Howard, T.A., Deforest, C.E., 2012. The thomson surface. I. Reality and myth. Astrophysical Journal 752, 130. doi:10.1088/0004-637X/752/2/130.

Jones, G.H., Knight, M.M., Battams, K., Boice, D.C., Brown, J., Giordano, S., Raymond, J., Snodgrass, C., Steckloff, J.K., Weissman, P., Fitzsimmons, A., Lisse, C., Opitom, C., Birkett, K.S., Bzowski, M., Decock, A., Mann, I., Ramanjooloo, Y., McCauley, P., 2018. The Science of Sungrazers, Sunskirters, and Other Near-Sun Comets. Space Science Reviews 214, 20. doi:10.1007/s11214-017-0446-5.

Koutchmy, S., Lamy, P., 1978. Propagating inhomogeneities in the dust tail of comet west 1975. Nature 273, 522–524. doi:10.1038/273522a0.

Kramer, E.A., Fernandez, Y.R., Lisse, C.M., Kelley, M.S., Woodney, L.M., 2014. A dynamical analysis of the dust tail of Comet C/1995 O1 (Hale–Bopp) at high heliocentric distances. Icarus 236, 136–145. doi:10.1016/j.icarus.2014.03.033.

Lamy, P.L., Koutchmy, S., 1979. Comet West 1975n. II - Study of the striated tail. Astron. & Astroph. 72, 50–54.

Lang, D., Hogg, D.W., Mierle, K., Blanton, M., Roweis, S., 2010. Astrometry. net: Blind astrometric calibration of arbitrary astronomical images. The Astronomical Journal 139, 1782.

McClure, A., 1962. Latest Pictures of Comet Seki-Lines. Sky & Telescope 23.

Mendis, D., Horányi, M., 2013. Dusty plasma effects in comets: Expectations for rosetta. Reviews of Geophysics 51, 53–75. doi:10.1002/rog.20005.

Morgan, H., Druckmüller, M., 2014. Multi-scale gaussian normalization for solar image processing. Solar Physics 289, 2945–2955. doi:10.1007/s11207-014-0523-9.

Müller, D., St. Cyr, O.C., Zouganelis, I., Gilbert, H.R., Marsden, R., Nieves-Chinchilla, T., Antonucci, E., Auchère, F., Berghmans, D., Horbury,

T.S., Howard, R.A., Krucker, S., Maksimovic, M., Owen, C.J., Rochus, P., Rodriguez-Pacheco, J., Romoli, M., Solanki, S.K., Bruno, R., Carlsson, M., Fludra, A., Harra, L., Hassler, D.M., Livi, S., Louarn, P., Peter, H., Schühle, U., Teriaca, L., del Toro Iniesta, J.C., Wimmer-Schweingruber, R.F., Marsch, E., Velli, M., De Groof, A., Walsh, A., Williams, D., 2020. The Solar Orbiter mission. Astronomy & Astrophysics 642, A1. URL: https://www.aanda.org/10.1051/0004-6361/202038467, doi:10.1051/0004-6361/202038467.

Mumford, S.J., Freij, N., Christe, S., Ireland, J., Mayer, F., Stansby, D., Shih, A.Y., Hughitt, V.K., Ryan, D.F., Liedtke, S., Pérez-Suárez, D., I., V.K., Hayes, L., Chakraborty, P., Inglis, A., Pattnaik, P., Sipőcz, B., Sharma, R., Leonard, A., Hewett, R., Barnes, W., Hamilton, A., Manhas, A., Panda, A., Earnshaw, M., Choudhary, N., Kumar, A., Singh, R., Chanda, P., Haque, M.A., Kirk, M.S., Mueller, M., Konge, S., Srivastava, R., Jain, Y., Bennett, S., Baruah, A., Arbolante, Q., Maloney, S., Charlton, M., Mishra, S., Paul, J.A., MacBride, C., Chorley, N., Himanshu, Chouhan, A., Modi, S., Sharma, Y., Mason, J.P., Naman9639, Zivadinovic, L., Bobra, M.G., Rozo, J.I.C., Manley, L., Ivashkiv, K., Chatterjee, A., von Forstner, J.F., Bazán, J., Stern, K.A., Evans, J., Jain, S., Malocha, M., Ghosh, S., Stańczak, D., SophieLemos, Singh, R.R., Visscher, R.D., Verma, S., Airmansmith97, Buddhika, D., Sharma, S., Pathak, H., Rideout, J.R., Agrawal, A., Alam, A., Bates, M., Park, J., Shukla, D., Mishra, P., Dubey, S., Taylor, G., Dacie, S., Jacob, Goel, D., Sharma, D., Inchaurrandieta, M., Cetusic, G., Reiter, G., Zahniy, S., Sidhu, S., Bray, E.M., Meszaros, T., Eigenbrot, A., Surve, R., Parkhi, U., Robitaille, T., Pandey, A., Price-Whelan, A., J, A., Chicrala, A., Ankit, Guennou, C., D'Avella, D., Williams, D., Verma, D., Ballew, J., Murphy, N., Lodha, P., Bose, A., Augspurger, T., Krishan, Y., honey, neerajkulk, Altunian, N., Ranjan, K., Bhope, A., Molina, C., Gomillion, R., Kothari, Y., Streicher, O., Wiedemann, B.M., Mampaey, B., Nomiya, Y., mridulpandey, Habib, I., Letts, J., Agarwal, S., Gaba, A.S., Hill, A., Keşkek, D., Kumar, G., Verstringe, F., Dover, F.M., Tollerud, E., Arias, E., Srikanth, S., Jain, S., Stone, B., Kustov, A., Smith, A., Sinha, A., Kannojia, S., Mehrotra, A., Yadav, T., Paul, T., Wilkinson, T.D., Caswell, T.A., Braccia, T., Pereira, T.M.D., Gates, T., yasintoda, Dang, T.K., Wilson, A., Bankar, V., Bahuleyan, A., B, A., platipo, Stevens, A.L., Gyenge, N.G., Schoentgen, M., Shahdadpuri, N., Dedhia, M., Mendero, M., Cheung, M., Agrawal, Y., Mangaonkar, M., Lyes, M.M., resakra, Ghosh, K., Hiware, K., Chaudhari, K., Mekala, R.R., Krishna, K., Buitrago-Casas, J.C., Das, R., Mishra, R., Sharma, R., Wimbish, J., Calixto, J., Babuschkin, I., Mathur, H., Murray, S.A., nakul shahdadpuri, 2022. Sunpy. URL: https://doi.org/10.5281/zenodo.5831717, doi:10.5281/zenodo.5831717.

Nishioka, K., 1998. Finite lifetime fragment model 2 for synchronic band formation in dust tails of comets. Icarus 134, 24–34.

Nishioka, K., 2021. Finite Lifetime Fragment Model 3 for striae formation in the dust tails of comets (FLM 3). Icarus 370, 114649. doi:10.1016/j.icarus.2021.114649.

Nishioka, K., Saito, K., Watanabe, J.I., Ozeki, T., 1992. Photographic observations of the synchronic band in the tail of Comet West 1976 VI. Publications of the National Astronomical Observatory of Japan 2, 601–621.

Nishioka, K., Watanabe, J.I., 1990. Finite lifetime fragment model for synchronic band formation in dust tails of comets. Icarus 87, 403–411.

Notni, P., Thaenert, W., 1988. The striae in the dust tails of great comets - A comparison to various theories. Astronomische Nachrichten 309, 133–146. doi:10.1002/asna.2113090210.

Pittichová, J., Sekanina, Z., Birkle, K., Boehnhardt, H., Engels, D., Keller, P., 1997. An Early Investigation Of The Striated Tail Of Comet Hale-Bopp (C/1995 O1). Earth, Moon, and Planets 78, 329–338. doi:10.1023/A:1006242209416.

Price, O., Jones, G.H., Morrill, J., Owens, M., Battams, K., Morgan, H., Drückmuller, M., Deiries, S., 2019. Fine-scale structure in cometary dust tails I: Analysis of striae in Comet C/2006 P1 (McNaught) through temporal mapping. Icarus 319, 540–557.

Ramanjooloo, Y., 2015. Comets as natural laboratories: Interpretations of the structure of the inner heliosphere. Ph.D. thesis. University College London.

Ramanjooloo, Y., Jones, G.H., 2022. Solar wind velocities at comets c/2011 l4 pan-starrs and c/2013 r1 lovejoy derived using a new image analysis technique. Journal of Geophysical Research: Space Physics 127, e2021JA029799. doi:10.1029/2021JA029799.

Raouafi, N.E., Lisse, C.M., Stenborg, G., Jones, G.H., Schmidt, C.A., 2015. Dynamics of HVECs emitted from comet C/2011 L4 as observed by STEREO. Journal of Geophysical Research A: Space Physics 120, 5329–5340. doi:10.1002/2014JA020926, arXiv:1507.02579.

Schrijver, C.J., Siscoe, G.L., 2009. Heliophysics: Plasma physics of the local cosmos. Cambridge University Press.

Sekanina, Z., Farrell, J., 1980. The striated dust tail of comet west 1976 vi as a particle fragmentation phenomenon. The Astronomical Journal 85, 1538–1554.

Sekanina, Z, Farrell, J.A., 1982. Two dust populations of particle fragments in the striated tail of comet Mrkos 1957 V. Astronomical Journal 87, 1836. doi:10.1017/CBO9781107415324.004.

Sekenina, Z., Pittichová, J., 1997. Distribution law for particle fragmentation times in a theory for striated tails of dust comets: application to comet hale-bopp (c/1995 o1). Earth, Moon, and Planets 78, 339–346.

Snodgrass, C., Jones, G.H., 2019. The European Space Agency's Comet Interceptor lies in wait. Nature Communications 10, 5418. URL: http://dx.doi.org/10.1038/s41467-019-13470-1 http://www.nature.com/articles/s41467-019-13470-1, doi:10.1038/s41467-019-13470-1.

Steckloff, J.K., Jacobson, S.A., 2016. The formation of striae within cometary dust tails by a sublimation-driven yorp-like effect. Icarus 264, 160–171.

The SunPy Community, Barnes, W.T., Bobra, M.G., Christe, S.D., Freij, N., Hayes, L.A., Ireland, J., Mumford, S., Perez-Suarez, D., Ryan, D.F., Shih, A.Y., Chanda, P., Glogowski, K., Hewett, R., Hughitt, V.K., Hill, A., Hiware, K., Inglis, A., Kirk, M.S.F., Konge, S., Mason, J.P., Maloney, S.A., Murray, S.A., Panda, A., Park, J., Pereira, T.M.D., Reardon, K., Savage, S., Sipőcz, B.M., Stansby, D., Jain, Y., Taylor, G., Yadav, T., Rajul, Dang, T.K., 2020. The sunpy project: Open source development and status of the version 1.0 core package. The Astrophysical Journal 890, 68–. URL: https://iopscience.iop.org/article/10.3847/1538-4357/ab4f7a, doi:10.3847/1538-4357/ab4f7a.

Wainscoat, R., Micheli, M., Wells, L., Holmes, R., Foglia, S., Vorobjov, T., Sostero, G., Guido, E., Sato, H., Williams, G., 2011. Comet C/2011 L4 (Panstarrs). International Astronomical Union Circular 9215, 1.

Yang, B., Keane, J., Meech, K., Owen, T., Wainscoat, R., 2014. Multi-wavelength observations of comet C/2011 L4 (Pan-STARRS). Astrophysical Journal Letters 784, 2–6. doi:10.1088/2041-8205/784/2/L23, arXiv:1402.5414.